doi:10.1093/brain/awy142 BRAIN 2018: 141; 1963–1980 | 1963

BRAIN
A JOURNAL OF NEUROLOGY

Insulin signalling promotes dendrite and synapse regeneration and restores circuit function after axonal injury

Jessica Agostinone,[1,2] Luis Alarcon-Martinez,[1,2] Clare Gamlin,[3] Wan-Qing Yu,[3] Rachel O. L. Wong[3] and Adriana Di Polo[1,2]

See Peterson and Benowitz (doi:10.1093/brain/awy165) for a scientific commentary on this article.

Dendrite pathology and synapse disassembly are critical features of chronic neurodegenerative diseases. In spite of this, the capacity of injured neurons to regenerate dendrites has been largely ignored. Here, we show that, upon axonal injury, retinal ganglion cells undergo rapid dendritic retraction and massive synapse loss that preceded neuronal death. Human recombinant insulin, administered as eye drops or systemically after dendritic arbour shrinkage and prior to cell loss, promoted robust regeneration of dendrites and successful reconnection with presynaptic targets. Insulin-mediated regeneration of excitatory postsynaptic sites on retinal ganglion cell dendritic processes increased neuronal survival and rescued light-triggered retinal responses. Further, we show that axotomy-induced dendrite retraction triggered substantial loss of the mammalian target of rapamycin (mTOR) activity exclusively in retinal ganglion cells, and that insulin fully reversed this response. Targeted loss-of-function experiments revealed that insulin-dependent activation of mTOR complex 1 (mTORC1) is required for new dendritic branching to restore arbour complexity, while complex 2 (mTORC2) drives dendritic process extension thus re-establishing field area. Our findings demonstrate that neurons in the mammalian central nervous system have the intrinsic capacity to regenerate dendrites and synapses after injury, and provide a strong rationale for the use of insulin and/or its analogues as pro-regenerative therapeutics for intractable neurodegenerative diseases including glaucoma.

1 Department of Neuroscience, University of Montreal, Montreal, Quebec H2X 0A9, Canada
2 University of Montreal Hospital Research Center (CR-CHUM), University of Montreal, Montreal, Quebec H2X 0A9, Canada
3 Department of Biological Structure, University of Washington, 1959 NE Pacific Street, Seattle, Washington, 98195, USA

Correspondence to: Adriana Di Polo, PhD
Department of Neurosciences
University of Montreal
CRCHUM, 900 Rue Saint-Denis
Tour Viger, Room R09.480
Montreal, Quebec H2X 0A9, Canada
E-mail: adriana.di.polo@umontreal.ca

Keywords: insulin; dendrite regeneration; retinal ganglion cell; mammalian target of rapamycin; optic nerve

Abbreviations: ERG = electroretinogram; mTOR = mammalian target of rapamycin; PhNR = photopic negative response; pSTR = positive scotopic threshold response; RGC = retinal ganglion cell

Received December 20, 2017. Revised March 21, 2018. Accepted April 6, 2018. Advance Access publication June 21, 2018

Introduction

Dendrites are exquisitely specialized processes that determine how neurons receive and integrate information within neuronal circuits. Dendrite retraction and synapse disassembly are early signs of pathology in a number of psychiatric and neurodegenerative disorders (Stephens *et al.*, 2005; Grutzendler *et al.*, 2007; Cochran *et al.*, 2014; Agostinone and Di Polo, 2015; Hong *et al.*, 2016; Yan *et al.*, 2016; Kweon *et al.*, 2017). Dendritic pathology occurs prior to soma or axon loss and correlates with substantial functional deficits (Cochran *et al.*, 2014). A critical question is whether dendrites from adult injured neurons can regenerate and reconnect with presynaptic targets once they have retracted. In mammals, CNS neurons have an extremely limited capacity to regenerate after injury (Aguayo *et al.*, 1990). While a large number of studies have focused on axonal regeneration (He and Jin, 2016; Benowitz *et al.*, 2017), the ability of mammalian neurons to regrow dendrites and re-establish functional synapses has been largely ignored. This is a critical issue because pathological disconnection from presynaptic targets leads to persistent functional impairment and accrued neuronal death.

Aberrant or insufficient insulin signalling, even in the absence of diabetes, has been associated with neurodegeneration in diseases characterized by dendritic pathology, notably Alzheimer's and Parkinson's disease, as well as glaucoma (Athauda and Foltynie, 2016; Song *et al.*, 2016; Bloom *et al.*, 2017). Traditionally viewed solely as a peripherally acting hormone, insulin crosses the blood–brain barrier and can influence a number of physiological brain processes including neuronal survival, neurotransmission, and cognitive performance (Ghasemi *et al.*, 2013). It has been suggested that insulin signalling may be potentially targeted for disease modification (Bedse *et al.*, 2015); however, its role in the response of vulnerable neurons is poorly understood. Along these lines, intranasal insulin administration has been reported to improve memory and attention in patients with Alzheimer's disease (Freiherr *et al.*, 2013), but the mechanism underlying this effect is currently unknown. Here, we asked whether insulin signalling promotes dendrite regeneration and the re-establishment of functional connections and, if so, which intracellular pathways regulate this response.

To address this, we focused on retinal ganglion cells (RGCs), a population of long-projecting CNS neurons that convey visual information from the retina to the brain via their axons in the optic nerve. The selective death of RGCs is a crucial element in the pathophysiology of glaucoma, the leading cause of irreversible blindness worldwide (Tham *et al.*, 2014). The rapid retraction of RGC dendrites is one of the earliest pathological changes in glaucoma (Agostinone and Di Polo, 2015). Insulin receptors are abundantly expressed by adult RGCs (Bu *et al.*, 2013), and impairment of insulin signalling in these neurons inhibits neurite outgrowth (Song *et al.*, 2015). Insulin binding to its receptor activates phosphoinositide-3′ kinase (PI3K) and its target Akt leading to potent activation of the mammalian target of rapamycin (mTOR) complexes 1 and 2 (mTORC1 and mTORC2) (Saxton and Sabatini, 2017). The mTORC1 multiprotein complex includes the core components mTOR, Raptor (regulatory protein associated with mTOR, encoded by *RPTOR*), and mLST8 (mammalian lethal with Sec13 protein 8) (Hara *et al.*, 2002; Kim *et al.*, 2003). Instead of Raptor, mTORC2 contains Rictor (rapamycin insensitive companion of mTOR, encoded by *RICTOR*), a completely unrelated protein that serves an analogous function (Dos *et al.*, 2004; Jacinto *et al.*, 2004).

Our data demonstrate that insulin, administered at a time when there is substantial dendritic arbour retraction, promotes remarkable dendrite regeneration. We show that activation of both mTORC1 and mTORC2 is essential for successful insulin-dependent dendritic regeneration. Furthermore, insulin treatment leads to striking regeneration of pre- and postsynaptic components, with marked increase in excitatory postsynaptic sites in ON-sustained, OFF-sustained, and OFF-transient RGCs. Importantly, insulin promoted robust neuronal survival and rescued light-triggered retinal responses. Together, our findings demonstrate that mammalian CNS neurons have the capacity to regenerate dendrites and synapses after injury, and identify the insulin-mTORC1/2 signalling pathway as a critical component for dendritic arbour repair and restoration of circuit function.

Materials and methods

Experimental design and animals

All animal procedures were approved by the Centre de Recherche du Centre Hospitalier de l'Université de Montréal (CRCHUM) Animal Care Committee, and followed the ARRIVE and the Canadian Council on Animal Care guidelines. Surgical procedures were carried out in B6.Cg.Tg[Thy1-YFPH]2Jrs/J mice (Jackson Laboratory) or wild-type littermate controls (3–4 months of age) maintained under 12-h light/12-h dark cyclic light conditions with an average in-cage illumination level of 10 lx. All experiments were performed under general anaesthesia using 2% isoflurane (0.8 l/min), except for electroretinogram (ERG) recordings (see below). The number of animals used in each experiment is indicated in the tables and in the figure legends. Data analysis was always carried out blinded by third party concealment of treatment using uniquely coded samples.

Optic nerve axotomy

Axonal injury was induced by complete transection (axotomy) of the optic nerve to trigger rapid and stereotypical loss of RGCs (Alarcón-Martínez *et al.*, 2010; Galindo-Romero *et al.*, 2011). Briefly, an incision in the skin over the superior orbital rim was made to gain access to the back of the eye. The

dural sheath was longitudinally opened to expose the optic nerve, which was then cleanly transected at 0.5–1 mm from the optic nerve head. Care was taken not to damage the central retinal artery, and fundus examination was routinely performed before and after the procedure to verify the integrity of the retinal circulation. Animals showing compromised blood supply were excluded from the study. Axotomy can induce changes in the contralateral eye (Ramírez *et al.*, 2015) therefore, with the exception of ERG recordings (see below), all control eyes in this study were from naïve, non-injured animals.

Retinal immunohistochemistry

Animals were deeply anaesthetized and transcardially perfused with 4% paraformaldehyde (PFA). The eyes were immediately collected and the retinas were dissected out. For flat-mount preparations, the retinas were free-floated for 3 days in 2% Triton^{TM} X-100 and 0.5% dimethyl sulphoxide (DMSO) in phosphate-buffered saline (PBS), followed by incubation for 2 h in blocking solution [10% normal goat serum (NGS), 2% Triton^{TM} X-100, 0.5% DMSO]. The following primary antibodies were applied and incubated overnight at 4°C: SMI-32 (NF-H, 10 µg/ml, Sternberger Monoclonals) or GFP (4 µg/ml, Sigma-Aldrich). Retinas were washed and incubated with secondary antibodies: anti-mouse Alexa Fluor® 594 (2 µg/ml, Molecular Probes) or anti-rabbit Alexa Fluor® 488 (2 µg/ml, Molecular Probes). For retinal cross sections, eyes were embedded in optimal cutting temperature (O.C.T.) compound and cryosections (12 µm) were prepared (Lebrun-Julien *et al.*, 2009). Sections were incubated overnight at 4°C in the following primary antibodies: phospho-S6 (Ser$^{240/244}$, 1:200, Cell Signaling Technology) and RNA binding protein with multiple splicing (RBPMS, 1:1000, Phosphosolutions), followed by secondary anti-guinea pig or anti-rabbit antibodies (Alexa 594 or 488, 2 µg/ml, Molecular Probes). Three retinal cross sections per eye were analysed at two areas (central and peripheral) for a total of six output measures per mouse. Samples were mounted and visualized with a Zeiss AxioSkop 2 Plus microscope (Carl Zeiss).

Dendritic arbour analysis

Dendritic arbour reconstruction and measurements were performed blinded to manipulations. High-resolution images of yellow fluorescent protein (YFP)-labelled RGC dendrites were acquired using a confocal microscope (Leica Microsystems Inc.). Scans were taken at 0.5 µm intervals (1024 × 1024 pixels) with an average of three to five images per focal plane. Reconstruction of dendritic trees was carried out using the computer-aided filament tracing function of Imaris (Bitplane). The following parameters were measured: (i) total dendritic length: the sum of the lengths of all dendrites per neuron; (ii) total dendritic field area: the area within the contour of the arbour created by drawing a line connecting the outermost tips of the distal dendrites; (iii) total number of branches: the sum of all dendritic branches per neuron; and (iv) Sholl analysis: the number of dendrites that cross concentric circles at increasing distances (10-µm interval) from the soma. RGCs located in all retinal quadrants and eccentricities were included in our analysis.

Insulin and drug administration

Human recombinant insulin diluted in sterile, endotoxin free PBS (15–30 U/kg/day, Sigma-Aldrich; or Humulin-R U100, Eli Lilly) was administered by daily intraperitoneal (i.p.) injections or eye drops (5 µl drop) as per the regimen outlined in Fig. 1F.

For topical delivery, the permeation enhancer polyoxyethylene-20-oleyl ether was added to the insulin solution (0.5%, Brij93, Sigma-Aldrich). Control animals received daily intraperitoneal or eye drops of vehicle. No allergic response, inflammation, or side-effects were detected, as previously reported in humans (Bartlett *et al.*, 1994). Recombinant FITC-tagged insulin (Sigma-Aldrich) was used to examine insulin access to retinal tissue. The dual mTORC1/2 inhibitor KU0063794 (8 mg/kg/day, i.p., Tocris Bioscience) (Zhang *et al.*, 2013), which crosses the blood–retinal barrier, was administered alone or in combination with insulin. Rapamycin (6 mg/kg, LC Laboratories) was administered by intraperitoneal injection.

Short interfering RNA sequences and intravitreal delivery

The following short interfering RNA (siRNA) sequences against *RPTOR*/Raptor and *RICTOR* were purchased from Dharmacon (ON-TARGET plus, Smartpool GE Dharmacon) (sense strands). *RPTOR*/Raptor: (i) 5′- UAG AGGUAGCU GCGAUUAA-3′; (ii) 5′-AUACUGACCGGGAGACGAA-3′; (iii) 5′- AGAAUGAAGGAUCGGAU GA-3′; and (iv) 5′-CUG AGGAACACUCGAGUCA-3′; *RICTOR*: (i) 5′-CUUAGAAG AUCUCGUGAAA-3′; (ii) 5′-AUGUAGAAUUAGAGCGAAU-3′; (iii) 5′-CAUUAAUUGCGGUUGGAAA-3′; and (iv) 5′-CGAUAUUG GCCAUAGUGAA-3′. A non-targeting siRNA was used as control (siCtl, ON-TARGET plus, Smartpool, GE Dharmacon). In some experiments a non-targeting Cy3-tagged control siRNA (siCtl-Cy3) was used to visualize siRNA uptake by retinal cells (Thermo Fisher Scientific). Each siRNA pool (7 µg/µl, total volume: 2 µl) was injected into the vitreous chamber of the eye using a custom-made glass microneedle (Wiretrol II capillary, Drummond Scientific Co). Under general anaesthesia, the sclera was exposed and the tip of the needle inserted into the superior ocular quadrant at a 45° angle through the sclera and retina into the vitreous space. This route of administration avoided injury to the iris or lens, which can promote RGC survival (Mansour-Robaey *et al.*, 1994; Leon *et al.*, 2000).

Western blot analysis

Whole retinas were rapidly isolated and homogenized in ice-cold lysis buffer: 150 mM NaCl, 20 mM Tris, pH 8.0, 1% NP-40, 0.5% Na deoxycholate, 0.1% SDS, 1 mM EDTA, supplemented with 2 mM $NaVO_3$, and protease and phosphatase inhibitors. Protein samples were resolved on SDS polyacrylamide gels and transferred to nitrocellulose membranes (Bio-Rad Life Science). Blots were incubated with each of the following antibodies: phospho-Akt (Ser^{473}, 1:2000, Cell Signaling Technology), total Akt (1:2000, Cell Signaling Technology), Rictor (1:2000, Thermo Fisher Scientific), Raptor (0.96 µg/ml, Abcam), or β-actin (0.5 µg/ml, Sigma-Aldrich), followed by anti-rabbit or anti-mouse peroxidase-linked secondary antibodies (0.5 µg/ml, GE Healthcare). Densitometric

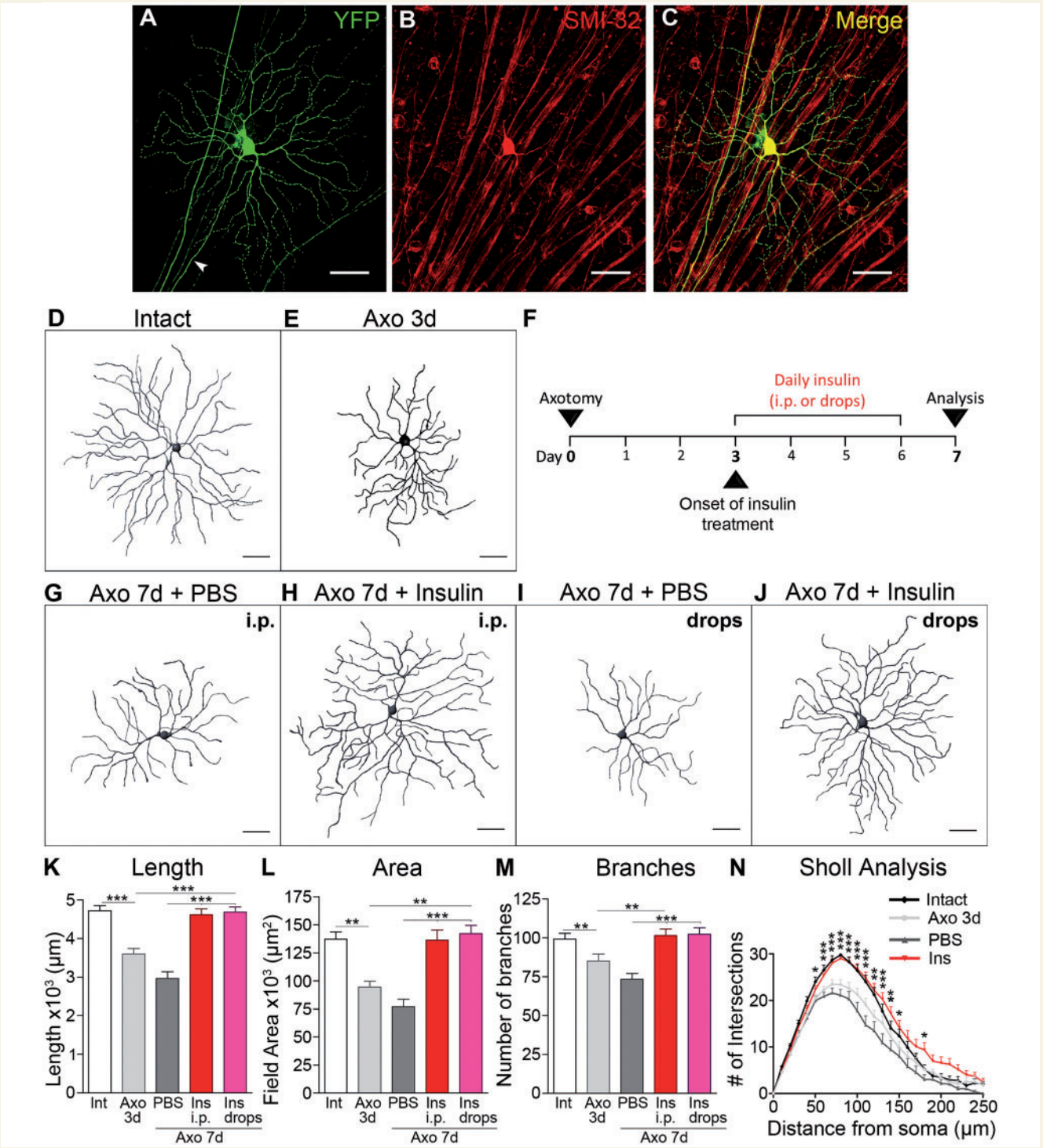

Figure 1 Insulin promotes dendritic regeneration in adult RGCs after axonal injury. (**A**–**C**) RGCs co-expressing YFP and SMI-32 (NF-H) with a clearly identifiable axon (arrowhead) were selected for dendritic arbour imaging and 3D reconstruction. (**D** and **E**) Three days after axotomy, RGCs had visibly smaller and simpler dendritic arbours relative to intact, non-injured neurons. (**F**) Human recombinant insulin or vehicle (PBS) were administered daily for four consecutive days by intraperitoneal injection (i.p.) or topically (eye drops) starting at 3 days post-axotomy, a time when there is already substantial dendrite retraction. RGC dendritic arbour analysis was carried out 7 days after injury. (**G**–**J**) Representative examples of dendritic arbours from axotomized retinas treated with vehicle or insulin, following the regimen described in (**F**), visualized at 7 days post-lesion (4 days of insulin treatment). (**K**–**N**) Quantitative analysis of dendritic parameters revealed that insulin-treated neurons had longer dendrites and markedly larger and more complex arbours than vehicle-treated controls (insulin i.p.: red, insulin eye drops: pink, PBS: dark grey). Values are expressed as the mean ± SEM. (ANOVA, ***$P < 0.001$, **$P < 0.01$, *$P < 0.05$, n = 4–6 mice/group, n = 28–46 RGCs/group, Table 1). The number of cells analysed in each group is indicated in Table 1. Scale bars: **A**–**C** = 25 µm, **E**–**J** = 50 µm.

analysis was performed using ImageJ (http://imagej.nih.gov/ij/) on scanned autoradiographic films obtained from five independent western blots, each carried out using retinal samples from different experimental groups.

Analysis of synaptic markers on retinal cross-sections

Mice were sacrificed by decapitation under deep anaesthesia (5% isoflurane), and the eyes were immediately collected. The cornea was carefully pierced with a 30-gauge needle and the eye was incubated in ice-cold 4% carbodiimide (Thermo Fisher Scientific) for 30 min. Retinal cryosections (16 µm) were generated and incubated with each of the following primary antibodies overnight at 4°C: VGLUT1 (1:800, Synaptic System) and PSD95 (2 µg/ml, Abcam). Sections were washed and incubated with secondary antibodies: anti-guinea pig and anti-mouse (Alexa 594 or 488, 2 µg/ml, Molecular Probes). Three retinal cross sections per eye were analysed at two areas (central and peripheral) for a total of six output measures per mouse. Fluorescent labelling was visualized with a Leica SP5 confocal microscope (Leica Microsystems Inc.), and 7.5-µm thick *z*-stacks were sequentially obtained at 0.13-µm intervals (1024 × 1024 pixels) with an average of three images per focal plane. Quantitative analysis of voxels, which measured the 3D volume occupied by pre- and postsynaptic markers, was carried out using Imaris (ImarisColoc, Bitplane). VGLUT1 and PSD95 did not co-localize in the same structure, but some overlap was detected due to light diffraction-limited resolution.

Biolistic gene delivery and analysis of excitatory postsynaptic site density

Mice were deeply anaesthetized, killed by cervical dislocation, and the eyes were immediately collected in oxygenated mouse artificial CSF (119 mM NaCl, 2.5 mM KCl, 1.3 mM $MgCl_2$, 2.5 mM $CaCl_2$, 1 mM $NaHPO_4$, 11 mM glucose, 20 mM HEPES, pH 7.4). Retinas were quickly dissected out and flat-mounted onto nitrocellulose filter paper (Millipore Corporation). Gold particles (12.5 mg, 1.6 µm, Bio-Rad) were coated with CMV:tdTomato (20 µg) and CMV:PSD95-YFP (7 µg) DNA plasmids. A Helios gene gun (Bio-Rad) was used to biolistically deliver the DNA-coated gold particles to whole-mounted retinas, which were then transferred to an oxygenated humidified chamber and maintained for 24 h at 32°C (Della Santina *et al.*, 2013; Ou *et al.*, 2016). Samples were fixed in 4% PFA, mounted, and images were acquired using a Leica SP5 confocal microscope (0.120 × 0.120 × 0.294 µm). RGCs were classified according to their dendritic arbour morphology and stratification level in the inner plexiform layer, defined as the distance between the RGC soma and the plane of dendrite ramification. Dendritic arbours and PSD95 puncta were 3D reconstructed and analysed using the Imaris filament tracing and dot finding functions (Bitplane). Candidate puncta present in only one confocal plane or <0.25 µm in diameter were not included in our analysis (Della Santina *et al.*, 2013; Ou *et al.*, 2016).

Electroretinography

Animals were dark adapted overnight prior to ERG recordings and all manipulations were carried out under dim red light. Mice were anaesthetized by intraperitoneal injection of ketamine (20 mg/kg, Bimeda), xylazine (2 mg/kg, Bayer), and acepromazine (0.4 mg/kg, Vétoquinol). Bilateral pupil dilation was induced by applying tropicamide on the cornea (1%, Mydriacyl®, Alcon). The intensity of the stimuli was calibrated using a dual-biosignal generator device adapted for ERG responses. The recording system used Burian-Allen bipolar electrodes adapted for use in mice. The active electrode, which has a corneal contact shape, was placed on the cornea following application of a drop of hydroxypropyl methylcellulose (Isopto® Tears, 0.5%, Alcon). The reference electrode was placed behind the ears, and the ground electrode in the tail. Electrical signals generated in the retina were amplified (1000×) and filtered (band-pass filter: 1–1000 Hz) using a commercial amplifier (Power Lab, ADInstruments). The recorded signals were digitized (Power Lab, ADInstruments) and displayed on a computer. Bilateral ERG recordings were performed simultaneously from both eyes. Measurements from non-injured naïve eyes (pre-injury) served as baseline, and contralateral eyes were used for data normalization. The ERG responses were recorded by stimulating the retina with light intensities ranging between 10^{-6} and 10^{-4} cd s/m^2 for the scotopic threshold response (STR), and 10^2 cd s/m^2 for the photopic negative response (PhNR). For each light intensity, a series of responses per flash were averaged (50 recordings). The interval between light flashes was adjusted to allow for response recovery. A calibration protocol was established to ensure homogenous stimulation and recording parameters and was performed immediately prior to each experiment.

Quantification of neuronal survival

Mice were subjected to transcardial perfusion with 4% paraformaldehyde and retinas were dissected out and fixed for an additional 15 min. Free-floating retinas were blocked overnight at 4°C in 10% normal goat serum, 2% bovine serum albumin, 0.5% Triton™ X-100 in PBS, and incubated with the RGC-specific marker RBPMS (1:1000, PhosphoSolutions) for 5 days at 4°C. Retinas were then incubated with Alexa 488-coupled secondary antibody (2 µg/ml, Molecular Probes) for 4 h at room temperature, mounted with the nerve fibre layer side up, and visualized with a Zeiss Axio Observer (Carl Zeiss). RBPMS-labelled RGCs were counted within three square areas at distances of 0.25, 0.625 and 1 mm from the optic nerve disc in each of the four retinal quadrants for a total of 12 retinal areas.

Statistical analysis

Data analysis and statistics were performed using GraphPad Instat software (GraphPad Software Inc., San Diego, CA) by a one-way analysis of variance (ANOVA) followed by a Bonferroni or Tukey *post hoc* tests, or by a Student's *t*-test as indicated in the legends.

Table 1 Dendritic parameters in experimental and control groups (data shown in Figs 1–3)

Condition	Total dendritic length, µm Mean ± SEM	Dendritic field area, µm^2 Mean ± SEM	Dendritic branches, *n* Mean ± SEM	Animals, *n*	RGCs, *n*
Intact	4718 ± 130 (100%)	137 284 ± 6451 (100%)	99 ± 4 (100%)	5	43
Axo 3 days	3598 ± 142	94 632 ± 5140	85 ± 5	4	28
Axo 7 days + PBS	2961 ± 180	77025 ± 6637	73 ± 4	5	32
Axo 7 days + Ins (i.p.)	4612 ± 156 (98%)	136 343 ± 9021 (99%)	101 ± 4 (102%)	6	46
Axo 7 days + PBS (drops)	2781 ± 80	80 673 ± 3736	64 ± 3	4	31
Axo 7 days + Ins (drops)	4677 ± 135 (99%)	142 063 ± 7520 (103%)	102 ± 4 (103%)	5	44
Axo 7 days + Ins + siCtl	4585 ± 155	145 340 ± 9600	100 ± 3	4	39
Axo 7 days + Ins + siRaptor	4115 ± 138	136 243 ± 6847	71 ± 2	5	43
Axo 7 days + Ins + siRictor	3138 ± 144	79 132 ± 5394	98 ± 5	5	43
Axo 7 days + Ins + KU	2649 ± 108	66 964 ± 3692	65 ± 3	4	38
Intact + KU	4758 ± 145	135 612 ± 6716	99 ± 4.3	4	41
Intact + siRaptor	4625 ± 131	138 960 ± 5784	97 ± 4.22	3	31
Intact + siRictor	4753 ± 182	150 757 ± 12 470	98 ± 5.13	3	25

Axo = axonal injury; KU = KU0063794; siCtl = control siRNA; siRaptor = siRNA against Raptor.

Results

Insulin promotes robust dendrite regeneration in adult RGCs after axonal injury

To investigate whether adult neurons have the capacity to regenerate dendrites, we used a well-characterized model of acute optic nerve transection to selectively damage RGC axons in transgenic mice expressing YFP under control of the *Thy1* promoter (Thy1-YFPH) (Feng *et al.*, 2000). Anatomical and functional studies have identified 15 to 32 RGC subtypes (Sun *et al.*, 2002; Coombs *et al.*, 2006; Volgyi *et al.*, 2009; Baden *et al.*, 2016), many of which are present in the Thy1-YFPH retina. The antibody SMI-32, which recognizes non-phosphorylated neurofilament heavy chain, was used to identify alpha RGCs characterized by strongly labelled somata and large dendritic arbours (Bleckert *et al.*, 2014; Baden *et al.*, 2016). YFP-positive RGCs that co-labelled with SMI-32 and had a clearly identifiable axon were selected for dendritic arbour imaging and 3D reconstruction (Fig. 1A–C). At 3 days after axotomy, dendrites had visibly retracted relative to non-injured, intact neurons (Fig. 1D and E). Analysis of total dendritic length and total dendritic area demonstrated a reduction of 23% and 31%, respectively, compared to intact SMI-32-positive RGCs (ANOVA $P < 0.001$, Table 1). Dendritic shrinkage occurred prior to RGC soma or axon loss, which starts at 5 days post-lesion in this model (Morquette *et al.*, 2015).

Based on the marked injury-induced dendritic retraction observed at 3 days, we initiated administration of human recombinant insulin or vehicle (PBS) at this time point and analysed dendritic length, area, and complexity 4 days later (7 days post-lesion). The insulin administration regimen shown in Fig. 1F, consisting of a daily dose of insulin over the course of 4 days starting at Day 3 after axotomy, was used for all the experiments in this study. Insulin was delivered by intraperitoneal injection, which led to mild and transient reduction in blood glucose levels followed by a quick recovery, or topically as eye drops with no detectable changes in glycaemia (Table 2). Dendritic arbour reconstruction and measurements were performed in RGCs co-labelled with YFP and SMI-32, and were always carried out blinded to treatments. At 7 days after axotomy, vehicle-treated RGCs displayed shrunken dendritic arbours with considerably fewer branches (Fig. 1G and I). In contrast, insulin administration, independently of delivery route, promoted robust RGC dendrite regeneration and restored process length, arbour area and complexity (Fig. 1H and J). For example, quantitative analysis of dendritic parameters following insulin treatment demonstrated a 36% increase in process length and 43% larger arbour area relative to vehicle-treated neurons (Fig. 1K and L, ANOVA $P < 0.001$ and $P < 0.01$, respectively, Table 1). Insulin also increased the number of dendritic branches relative to control neurons (Fig. 1M) and promoted a global surge in the number of branch intersections at all distances from the soma, as evidenced by Sholl analysis (Fig. 1N), suggesting enhanced arbour complexity. Overall, insulin restored all dendritic parameters to values similar to those in naïve uninjured retinas. Relative to intact retinas (100%), systemic insulin increased dendritic length, area, and branches to 98%, 99%, and 102%, respectively (Table 1). Similar dendritic regeneration was observed with topical insulin administration (Table 1). The observation that insulin delivered by two different routes, causing very small variations in blood glucose levels and yielding identical regenerative outcomes (Table 2 and Fig. 1H and J), rules out an effect of glycaemic changes on dendrite morphology. Administration of FITC-tagged recombinant insulin confirmed that insulin

Table 2 Blood glucose levels after insulin delivery

	Delivery route	Time after insulin administration (min)								
		0	60	120	180	240	300	360	420	480
Glycaemia, mmol/l	Systemic (i.p.) $n = 5$	6 ± 0.3	2.4 ± 0.3 ($P < 0.001$)	1.9 ± 0.1 ($P < 0.001$)	2.1 ± 0.1 ($P < 0.001$)	3.6 ± 0.2 ($P < 0.001$)	4.7 ± 0.2 ($P < 0.01$)	5.3 ± 0.4 (n.s.)	5.8 ± 0.1 (n.s.)	5.8 ± 0.3 (n.s.)
	Topical (drops) $n = 5$	5.6 ± 0.2	6.5 ± 0.5 (n.s.)	5.9 ± 0.6 (n.s.)	5.6 ± 0.5 (n.s.)	6.0 ± 0.8 (n.s.)	5.6 ± 0.5 (n.s.)	5.7 ± 0.5 (n.s.)	5.2 ± 0.3 (n.s.)	5.6 ± 0.3 (n.s.)

Data are shown as mean ± SEM. ANOVA, Dunnett's *post hoc* test, $n = 5$ mice/group, n.s. = not significant ($P > 0.05$).

effectively reached retinal cells (Supplementary Fig. 1). Collectively, these findings demonstrate that insulin, provided after dendrites have substantially retracted, promotes striking process regeneration and suggest that adult CNS neurons have the capacity to regrow dendrites after injury.

mTORC1 is required for insulin-mediated dendritic branching and restores arbour complexity

Insulin controls many aspects of cell growth and metabolism through activation of the mTOR pathway (Saxton and Sabatini, 2017). Recent evidence indicates that mTORC1 regulates dendritic arbour morphology (Morquette *et al.*, 2015; Skalecka *et al.*, 2016). To determine whether insulin-mediated RGC dendrite regeneration occurred through mTORC1 activation, we first examined whether dendritic retraction correlated with changes in endogenous mTORC1 activity in these neurons. mTORC1 activates the p70 ribosomal S6 kinase leading to phosphorylation of the ribosomal protein S6 at Ser240/244 residues ($pS6^{Ser240/244}$) thus stimulating protein translation (Jefferies *et al.*, 1997). Antibodies that recognize $pS6^{Ser240/244}$ are widely accepted functional readouts of mTORC1 function (Ikenoue *et al.*, 2009). Immunolabelling of non-injured retinas with $pS6^{Ser240/244}$ revealed two retinal cell populations with robust constitutive mTORC1 activity: one located in the ganglion cell layer and another in the inner nuclear layer (Fig. 2A). Co-labelling of $pS6^{Ser240/244}$ with RBPMS (RNA-binding protein with multiple splicing), a selective marker of RGCs (Rodriguez *et al.*, 2014), revealed robust mTORC1 activity in these neurons in the ganglion cell layer (Fig. 2B–D). A marked decrease of $pS6^{Ser240/244}$ in RGCs was detected at 4 days after axonal injury coinciding with early dendritic retraction, prior to the onset of neuronal death (Fig. 2E and H). Insulin treatment fully restored mTORC1 activity in injured RGCs, consistent with its ability to stimulate this signalling pathway (Fig. 2F and H). In the inner nuclear layer, $pS6^{Ser240/244}$ co-localized with the calcium-binding protein calbindin, a marker of horizontal cells (Supplementary Fig. 2A–C). In contrast to RGCs, $pS6^{Ser240/244}$ expression in horizontal cells remained unchanged after axotomy (Supplementary Fig. 2D–G), indicating RGC-specific mTORC1 downregulation in response to injury. The mTORC1 inhibitor rapamycin completely eliminated retinal pS6 labelling, thus supporting that pS6 is a true readout of mTOR function in this system (Supplementary Fig. 2H–K).

To determine whether insulin-induced activation of mTORC1 played a role in RGC dendrite regeneration, we sought to selectively reduce mTORC1 function. Rapamycin is an effective mTORC1 inhibitor (Chung *et al.*, 1992), but disrupts mTORC2 function and can induce insulin resistance (Sarbassov *et al.*, 2006; Lamming *et al.*, 2012). To avoid off-target effects of rapamycin, we selectively inhibited mTORC1 with a siRNA against Raptor, a specific and essential component of mTORC1 function (Schalm *et al.*, 2003). First, we examined whether siRNA delivered intraocularly was taken up by mouse RGCs. A single intravitreal injection of non-targeting Cy3-tagged control siRNA (siCtl-Cy3) resulted in RGC labelling as early as 3 h after administration (Supplementary Fig. 1L–O). The mechanism for this rapid preferential uptake is unknown, but it might relate to the ganglion cell layer being directly exposed to the vitreous chamber allowing rapid siRNA diffusion into RGCs.

Next, we assessed the ability of the siRNA against Raptor (siRaptor) to knockdown retinal Raptor protein expression and inhibit mTORC1 function. Retinal immunohistochemistry demonstrated that siRaptor decreased by ~50% the number of pS6-positive axotomized RGCs, visualized with RBPMS, following insulin treatment (ANOVA, $P < 0.001$, Fig. 2G and H). Western blot analysis confirmed that, in the presence of insulin, retinas that received siRaptor showed a significant reduction of Raptor protein, while non-targeting control siRNA (siCtl) had no effect (Fig. 2I and J). Importantly, siRaptor did not reduce the levels of Rictor, the analogous component in mTORC2 (Sarbassov *et al.*, 2004), validating the specificity of this siRNA (Fig. 2I and K).

We then asked whether siRaptor-mediated knockdown of mTORC1 function had an effect on insulin-induced RGC dendrite regeneration. For this purpose, siRaptor was intravitreally injected concomitantly with the onset of insulin administration (i.p.) at 3 days after optic nerve axotomy, and the neuronal morphology of RGCs co-labelled with YFP and SMI-32 was analysed 4 days later (7 days post-lesion, Fig. 1F). Mice received a single siRaptor intravitreal injection at the onset of daily insulin treatment. Our data show that insulin-mediated regeneration was partially

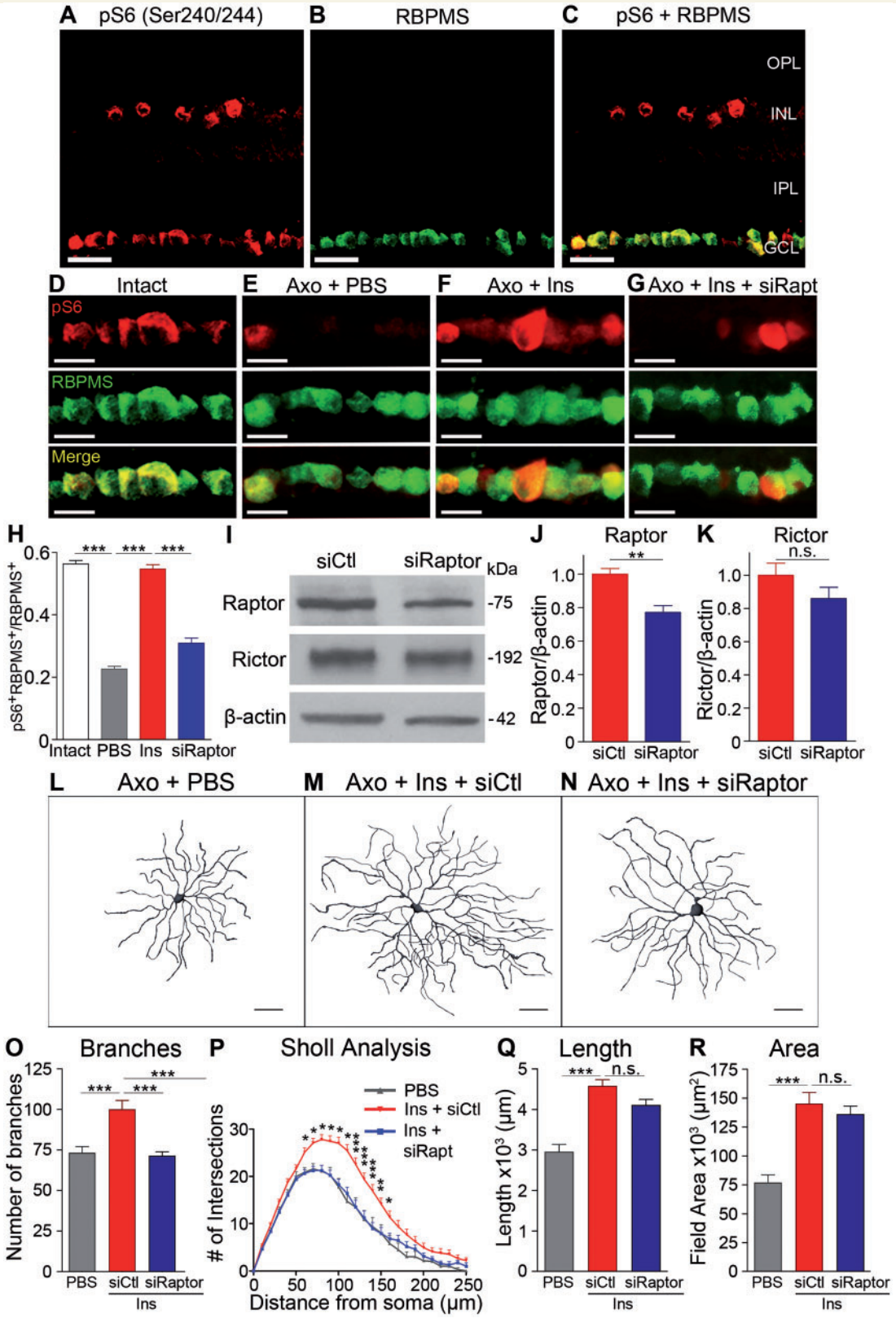

Figure 2 mTORC1 activity is required for insulin-mediated dendritic branching. (**A**–**D**) Immunohistochemical analysis of retinal cross sections with an antibody against pS6$^{Ser240/244}$, a readout of mTORC1 function, and RBPMS, a selective marker of RGCs, revealed robust mTORC1 activity in these neurons. (**E** and **F**) Axonal injury induced a marked decrease of pS6$^{Ser240/244}$ labelling in RGCs, suggesting loss of mTORC1 activity, which was restored by insulin treatment. (**G**) Co-administration of insulin with siRNA against Raptor (siRaptor), an essential component of mTORC1 function, blocked the effect of insulin on RGC-specific pS6$^{Ser240/244}$ levels. (**H**) Quantification of the number of cells expressing both pS6$^{Ser240/244}$ and RBPMS relative to all RBPMS-positive cells confirmed that insulin fully restored mTORC1 activity in injured

(continued)

blocked by siRaptor (Fig. 2L–N). A 30% reduction in the number of branches was observed with siRaptor, resulting in less complex arbours relative to non-targeting siCtl (Fig. 2O, red versus blue bars, ANOVA, $P < 0.001$, Table 1). Sholl analysis further confirmed a marked decrease in dendritic complexity in retinas treated with siRaptor (Fig. 2P). In contrast, the total dendritic length and arbour area were not affected by siRaptor-mediated blockade of mTORC1 function (Fig. 2Q and R and Table 1). Administration of siRaptor alone in non-injured retinas was not toxic and did not elicit changes in dendritic parameters (Table 1). Our data show that selective mTORC1 knockdown blocks the ability of insulin to increase the number of regenerating branches, suggesting that mTORC1 contributes to the restoration of arbour complexity.

mTORC2 regulates process extension and length in regenerating dendritic arbours

The partial inhibition of insulin-induced dendritic arbour regeneration observed in conditions of lower mTORC1 activity, prompted us to ask whether other signalling components participate in this response. In addition to mTORC1, insulin activates mTORC2 (Saxton and Sabatini, 2017). A critical role of mTORC2 is the phosphorylation of Akt, a key effector of insulin/PI3K signalling (Sarbassov *et al.*, 2005). mTORC2 phosphorylates Akt on Ser473 residues ($pAkt^{Ser473}$) in a Rictor- and mTOR-dependent manner (Sarbassov *et al.*, 2005), therefore we used antibodies against $pAkt^{Ser473}$ as a readout of mTORC2 activity. Western blot analysis of retinal homogenates demonstrated a substantial reduction of $pAkt^{Ser473}$ in axotomized retinas treated with vehicle, while insulin administration rescued $pAkt^{Ser473}$ levels (Fig. 3A and B), suggesting restoration of mTORC2 function. To establish the role of mTORC2 in insulin-mediated dendrite regeneration, we used an siRNA against Rictor (siRictor), a specific protein component essential for mTORC2 activity (Sarbassov *et al.*, 2004). In the presence of insulin, intraocular injection of siRictor resulted in effective depletion of retinal Rictor relative to non-targeting siCtl-treated eyes (Fig. 3C and D). Rictor knockdown resulted in $pAkt^{Ser473}$ downregulation indicative of mTORC2 function loss (Fig. 3C and E). Importantly, siRictor did not alter the levels of Raptor, thus validating its specificity (Fig. 3C and F).

To investigate whether mTORC2 played a role in insulin-mediated dendrite regeneration, siRictor and insulin were co-administered at 3 days after axotomy and dendritic arbours from YFP- and SMI32-positive RGCs were characterized 4 days later. Animals received a single siRictor intravitreal injection at the onset of daily insulin treatment (Fig. 1F). Loss of mTORC2 function impaired insulin-induced dendrite extension resulting in shorter dendrites and, consequently, considerably smaller arbour areas (Fig. 3G and H). Quantitative analysis of dendritic parameters confirmed 32% decrease in total dendritic length resulting in reduced surface coverage in eyes that received siRictor relative to non-targeting siCtl-treated controls (Fig. 3J and K, red versus black bars, ANOVA, $P < 0.001$, Table 1). Intriguingly, and contrary to what was observed with loss of mTORC1 function, decreased mTORC2 activity did not affect the number of branches or arbour complexity (Fig. 3H and L). Sholl analysis confirmed no significant changes in arbour complexity between retinas treated with insulin and siRictor or non-targeting siCtl (Fig. 3M).

Next, we asked whether mTORC1 and mTORC2 exerted additive roles in insulin-mediated dendritic regrowth. For this purpose, we co-administered insulin with KU0063794, a well-characterized cell permeable and selective dual inhibitor of mTORC1 and mTORC2 that does not affect other kinases (García-Martínez *et al.*, 2009), using the same regimen as above. Inhibition of both mTOR complexes completely abrogated insulin-mediated dendrite regeneration resulting in RGCs with rudimentary and shrivelled dendritic arbours, with shorter and considerably fewer processes, compared to control RGCs (Fig. 3I and J–L). Quantitative analysis confirmed that KU0063794 led to a dramatic reduction in total dendritic length, arbour area, and number of branches indicative of lower complexity (Fig. 3J–L, green bar and Table 1). Intraocular injection of KU0063794 alone in non-injured retinas did not induce cell toxicity or altered dendritic parameters (Table 1). Collectively, these data suggest that mTORC2 activity contributes to process extension and the re-establishment of arbour area, and that mTORC1 and mTORC2 play additive roles during insulin-induced dendrite regeneration.

Figure 2 Continued

RGCs relative to vehicle- or siRaptor-treated retinas (ANOVA, $^{***}P < 0.001$, $n = 5$ mice/group). (**I–K**) Western blot and densitometry analysis confirmed that intravitreal delivery of siRaptor reduced retinal Raptor protein while a non-targeting control siRNA (siCtl) had no effect (Student's *t*-test, $^{**}P < 0.05$, n.s. = not significant, $n = 6–7$ mice/group). siRaptor did not alter the levels of Rictor, confirming the specificity of the siRNA. The *lower* panel is the same blot as in the *upper* panel but probed with an antibody that recognizes β-actin to ensure equal protein loading. (**L–N**) Co-administration of insulin and siRaptor resulted in a marked loss of dendritic branches and simpler arbours relative to insulin alone or insulin combined with siCtl at 7 days post-injury. (**O–R**) Quantitative analysis of dendritic parameters, including Sholl analysis (**P**), confirmed that selective mTORC1 knockdown blocked the ability of insulin to increase the number of regenerating branches, while no significant changes in process length or arbour area were observed (**Q** and **R**) (ANOVA, $^{***}P < 0.001$, $^{**}P < 0.01$, $^{*}P < 0.05$, n.s. = not significant; $n = 4–5$ mice/group, $n = 32–43$ RGCs/group, Table 1). Values are expressed as the mean ± SEM. Scale bars: **A–C** and **L–N** = 50 μm, **D–G** = 25 μm. GCL = ganglion cell layer; INL = inner nuclear layer; IPL = inner plexiform layer; OPL = outer plexiform layer.

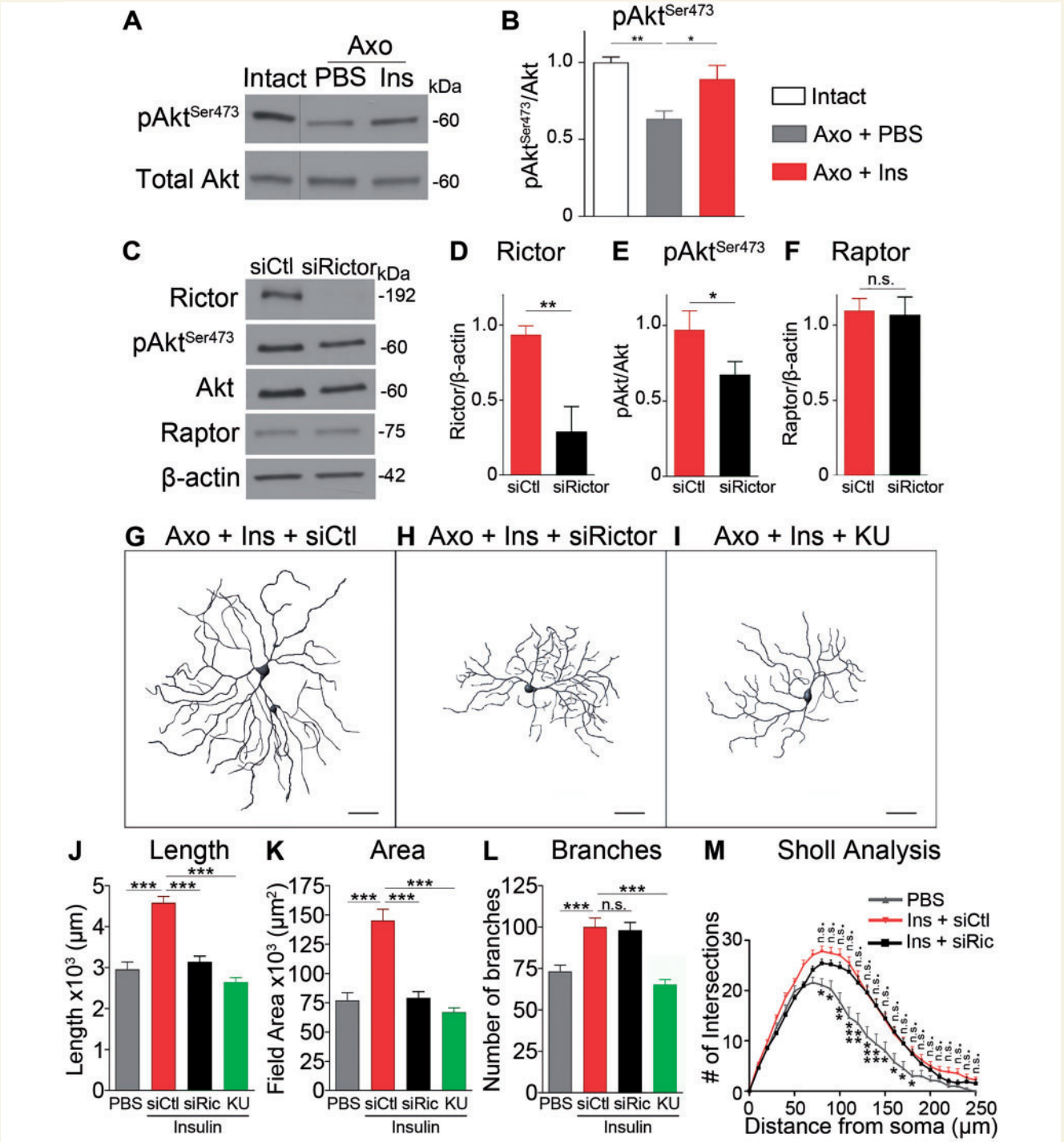

Figure 3 mTORC2 regulates process extension and length in regenerating dendritic arbours. (**A** and **B**) Western blot analysis of retinal homogenates demonstrated a substantial reduction of pAkt^{Ser473}, a readout of mTORC2 activity, in axotomized retinas treated with vehicle, while insulin administration rescued pAkt^{Ser473} levels (ANOVA, $^{**}P < 0.01$, $^{*}P < 0.05$, $n = 5$ mice/group). The *lower* panel is the same blot probed with an antibody against total Akt for normalization. (**C**–**F**) Western blot and densitometry analyses demonstrated that intravitreal injection of siRNA against Rictor (siRictor) led to reduction of retinal Rictor protein while a non-targeting control siRNA (siCtl) had no effect. Rictor knockdown also resulted in pAkt^{Ser473} downregulation, indicative of mTORC2 function loss, but did not alter the levels of Raptor, thus validating its specificity (Student's *t*-test, $^{**}P < 0.01$, $^{*}P < 0.05$, n.s. = not significant, $n = 6$–7 mice/group). The lowest panel represents the same blot probed with an antibody against β-actin to ensure equal protein loading. (**G** and **H**) Co-administration of insulin and siRictor resulted in a dramatic reduction in dendritic length and arbour area at 7 days post-injury relative to control retinas. (**I**) Administration of insulin and KU0063794 (KU), dual mTORC1 and mTORC2 inhibitor, resulted in overt dendrite degeneration characterized by a dramatic loss of branches and much shorter processes. Scale bars = 50 μm. (**J**–**M**) Quantitative analysis of dendritic parameters, including Sholl analysis (**M**), confirmed that siRictor-mediated mTORC2 inhibition resulted in a substantial loss of regenerating branches, while no significant changes in process length or arbour area were observed (ANOVA, $^{***}P < 0.001$, $^{**}P < 0.01$, $^{*}P < 0.05$, n.s. = not significant, $n = 4$–5 mice/group, $n = 38$–43 RGCs/group, Table 1). Values are expressed as the mean ± SEM.

Insulin restores glutamatergic postsynaptic sites in injured neurons

Excitatory inputs from bipolar cells onto RGCs occur at the ribbon synapse, a specialized structure that enables fast and sustained neurotransmission required for vision (Heidelberger *et al.*, 2005). We asked whether insulin restored glutamatergic synapses on regenerated dendritic processes. For this purpose, we first examined changes in endogenous vesicular glutamate transporter 1 (VGLUT1), a presynaptic protein expressed at bipolar ribbon synapses (Johnson *et al.*, 2003), and postsynaptic density protein 95 (PSD95) in the inner plexiform layer, where RGC dendrites are located. A pronounced decrease in the expression of both VGLUT1 and PSD95 was observed after axonal injury in vehicle-treated eyes relative to naïve controls (Fig. 4A and B). Insulin, administered after synapse disassembly according to the regimen shown in Fig. 1F, promoted marked rescue of VGLUT1 and PSD95 expression in the inner plexiform layer (Fig. 4C). Quantitative analysis of pre- and postsynaptic voxels, which measures the 3D volume occupied by VGLUT1 and PSD95 in the inner plexiform layer, confirmed that insulin promoted robust synaptic regeneration compared to vehicle-treated retinas (Fig. 4D–F, $n = 4$–6 mice/group).

To characterize the effect of insulin on the distribution of excitatory postsynaptic sites further, we used biolistic transfection of *CMV*:PSD95-YFP and *CMV*:tdTomato plasmids onto injured or control retinal whole mounts followed by analysis of PSD95 puncta on individual YFP-positive RGC dendrites (Fig. 4G). This technique has been previously validated for the analysis of excitatory postsynaptic site density in RGC dendritic branches (see 'Materials and methods' section) (Morgan *et al.*, 2008). Axotomized neurons had many varicosities along dendrites, often accompanied by large retraction bulbs at their tips (Fig. 4G), as well as larger PSD95 puncta size (Fig. 4H and I). A recent study suggested that OFF-transient RGCs are more prone to lose synapses in a mouse model of ocular hypertension glaucoma (Della Santina *et al.*, 2013), thus we analysed excitatory postsynaptic site density in ON-sustained OFF-sustained, and OFF-transient cells. RGC subtypes were classified according to their morphology and dendritic stratification level in the inner plexiform layer (Pang *et al.*, 2003; Huberman *et al.*, 2008; Van Wyk *et al.*, 2009) (Supplementary Fig. 3). Substantial dendritic alterations as well as marked loss of PSD95 puncta were observed in all alpha RGC subtypes following axotomy (Fig. 4J–U). Quantitative analysis of PSD95-YFP confirmed extensive synapse disassembly and loss of PSD95 puncta density in injured RGCs treated with vehicle, independently of subtype (Fig. 4K, O and S). Interestingly, although all alpha RGCs were affected, ON-sustained and OFF-transient RGCs displayed the highest vulnerability to axonal injury with a loss of ~65% of synapses when compared to non-injured RGCs (Fig. 4J, K, M, R, S and U; ANOVA, $P < 0.001$, $n = 3$–6 mice/group). Insulin promoted striking rescue of excitatory postsynaptic sites on RGC dendrites, again independently of subtype, returning PSD95 puncta to 76%, 93%, and 93% of control PSD95 densities on ON-sustained, OFF-sustained, and OFF-transient RGCs, respectively (Fig. 4L, M, P, Q, T and U, ANOVA, $P < 0.001$). We conclude that insulin restores postsynaptic site density on regenerating RGC dendrites.

Insulin rescues retinal function and increases neuronal survival

To assess the impact of insulin-mediated dendrite and synapse regeneration on RGC function, we measured two components of the full-field ERG: the pSTR and the PhNR. The pSTR and PhNR derive predominantly from RGC activity in the rodent retina, and are reduced after optic nerve injury and in glaucoma patients (Bui and Fortune, 2004; Alarcón-Martínez *et al.*, 2010; Chrysostomou and Crowston, 2013; Smith *et al.*, 2014; Wilsey and Fortune, 2016). Because of the non-invasive nature of the ERG, we longitudinally followed light responses in the same mice prior to axotomy, and after injury and administration of vehicle or insulin using the regimen outlined in Fig. 1F. Figure 5 shows representative pSTR and PhNR recordings from naïve retinas, prior to axotomy (Fig. 5A and D), and after lesion in mice treated with vehicle (Fig. 5B and E, PBS, blue trace) or insulin (Fig. 5C and F, red trace) relative to the contralateral non-injured eye (grey traces). Both the pSTR and PhNR responses were markedly reduced after optic nerve injury in vehicle-treated mice, with a 48% and 60% decrease in amplitude, respectively, relative to naïve eyes (Fig. 5G and H, ANOVA $P < 0.001$, $P < 0.05$, respectively). In contrast, insulin fully restored both the pSTR and PhNR amplitudes in injured retinas at 7 days post-axotomy (Fig. 5G and H, red bars, $n = 4$–10 mice/group) suggesting recovery of RGC function upon light stimulation. To rule out confounding secondary changes in the contralateral eye (Ramírez *et al.*, 2015), the contralateral control and experimental responses were compared. Our data show no significant differences between these responses (Supplementary Fig. 4) indicating that the contralateral eye was not affected in these conditions.

To investigate whether the pro-regenerative effect of insulin reflected on the ability of RGCs to survive after injury, we followed the same treatment regimen as above and analysed neuronal density on flat-mounted retinas at 1, 2, 4, and 6 weeks after axotomy. Retinas from eyes treated with insulin consistently showed higher densities of RBPMS-labelled RGCs than those treated with vehicle (Fig. 5I–L). Quantitative analysis demonstrated that insulin promoted substantial RGC survival relative to PBS-treated eyes at 1 week after optic nerve injury (insulin: 70% survival, vehicle: 46% survival, $n = 5$–6 mice/group, ANOVA $P < 0.001$) (Fig. 5M). Remarkably, insulin administration

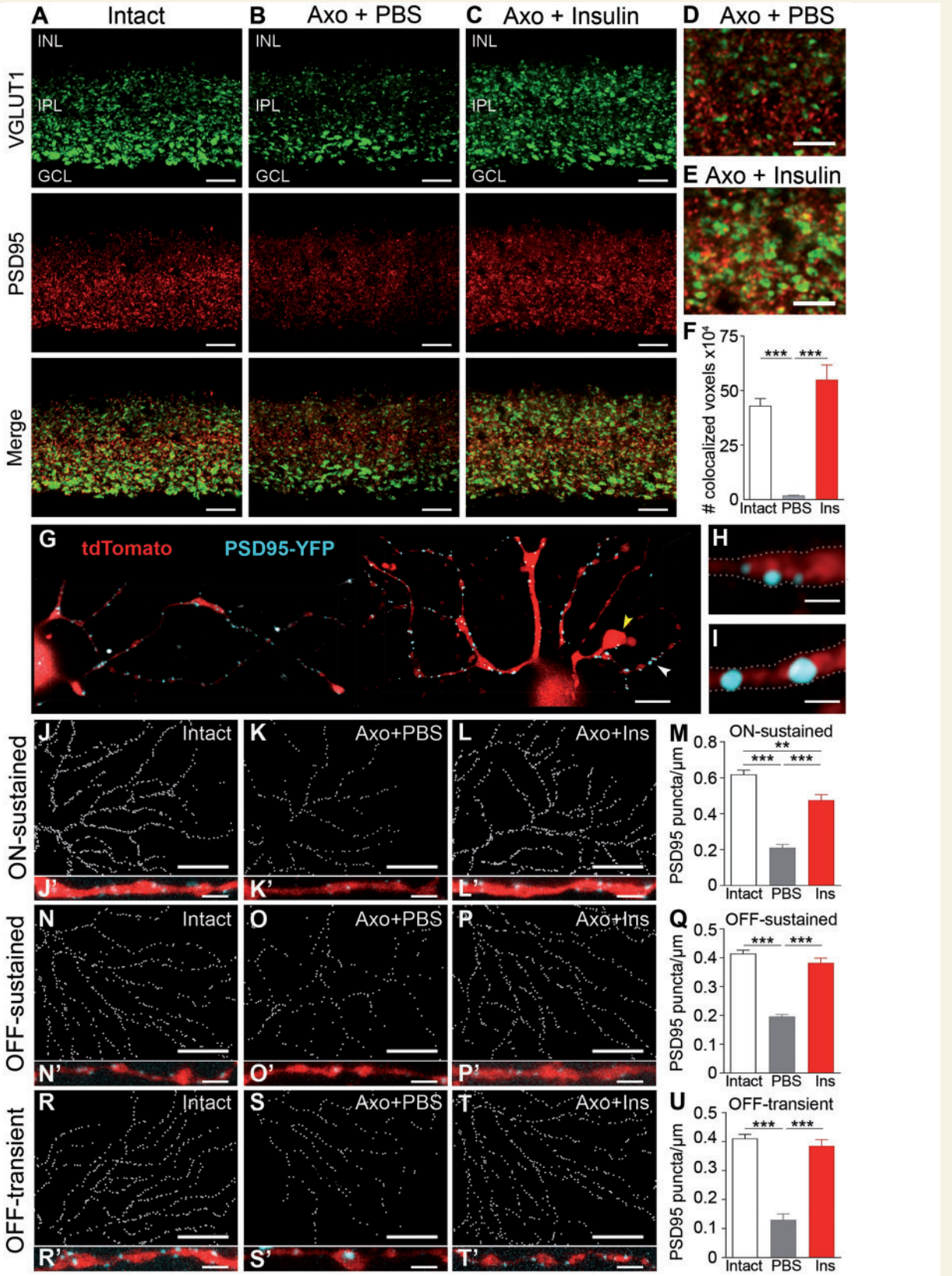

Figure 4 Insulin restores glutamatergic postsynaptic sites in injured neurons. (**A**) Glutamatergic synapses visualized in the inner plexiform layer (IPL) on retinal cross-sections using immunolabelling against VGLUT1 (green) and PSD95 (red), a pre- and a postsynaptic marker, respectively. (**B** and **C**) Axonal injury induced a pronounced loss of both VGLUT1 and PSD95 expression in the inner plexiform layer, which was completely restored by insulin treatment (analysis at 7 days post-axotomy). (**D** and **E**) High magnification of VGUT1 and PSD95 puncta in the inner plexiform layer at the level of the OFF sublamina in retinas treated with insulin or vehicle. (**F**) Quantitative analysis of pre- and postsynaptic

(continued)

resulted in sustained neuroprotection promoting the survival of 60% of RGCs at 2 weeks after injury, when only 14% of RBPMS-positive neurons remained in vehicle-treated eyes ($n = 5$–6 mice/group, ANOVA $P < 0.001$) (Fig. 5M). Furthermore, 25% of RGCs survived at 4 and 6 weeks, respectively, relative to 8% observed in vehicle treated controls (Fig. 5M, $n = 5$ mice/group, ANOVA $P < 0.05$ and $P < 0.01$, respectively). Next, we asked whether insulin-induced mTORC1 and mTORC2 activation played a role in neuronal survival. For this purpose, insulin was co-administered with KU0063794 and neuronal density was quantified at 1 and 2 weeks after axotomy. KU0063794 fully inhibited insulin-mediated neuroprotection, reducing the number of RGCs to levels similar to those found in vehicle-treated retinas (Fig. 5L and M). Administration of KU0063794 alone in intact, non-injured retinas did not alter RGC numbers, ruling out a toxic effect of this drug. Thus, insulin rescues RGC function and extends the survival of these neurons after axonal injury through mTOR signalling.

Discussion

Dendrites are extremely dynamic during development, elaborating and retracting rapidly in response to intrinsic and environmental cues (Wong and Wong, 2000; Cline, 2001), but they become stable in adulthood and undergo few structural changes thereafter (Koleske, 2013). The stability of dendrites is severely compromised following axonal injury or during neurodegeneration. Shrinkage of RGC dendritic arbours has been observed in primate, cat and rodent models of glaucoma (Weber *et al.*, 1998; Shou *et al.*, 2003; Morgan *et al.*, 2006; Li *et al.*, 2011; Della Santina *et al.*, 2013; Feng *et al.*, 2013; Williams *et al.*, 2013; Morquette *et al.*, 2015) as well as in human glaucomatous retinas (Pavlidis *et al.*, 2003; Fard *et al.*, 2016). Consistent with this, we show that selective injury to RGC axons triggers rapid dendritic shrinkage and loss of arbour complexity, prior to overt neuronal loss. Remarkably, insulin administration, after dendrite retraction had already occurred, promoted robust process regrowth and restoration of arbour area and complexity. Because our study focused on classic alpha RGCs expressing SMI-32, which are characterized by large somata and expansive dendritic fields with a typical branching pattern (Peichl, 1991), there is no risk of confounding retraction or lack of regeneration for neurons with more compact dendritic trees. Notably, spontaneous dendrite regeneration has been described in invertebrate systems. Peripheral nervous system sensory neurons in *Caenorhabditis elegans* and *Drosophila* display a robust ability to regrow the stereotypical pattern of dendritic branches after laser-induced dendrite ablation (Stone *et al.*, 2014; Thompson-Peer *et al.*, 2016; Oren-Suissa *et al.*, 2017). Recent work demonstrated the use of two-photon nanosurgery in the mouse brain to ablate single dendrites that resulted in rapid fragmentation of the distal end and formation of a retraction bulb (Zhao *et al.*, 2017). Using a prick-injury model in the cerebral cortex, another study showed dendritic regrowth by pyramidal cells after local injection of heparin-binding growth-associated molecule, an effect that was attributed to modification of the glial scar (Paveliev *et al.*, 2016). In our optic nerve injury model, RGC dendrites never regenerated unless they were stimulated with insulin, thus providing the first evidence of successful dendritic regeneration in retinal neurons. Failure to spontaneously regrow dendrites is reminiscent of the limited capacity for axonal regeneration in mammals relative to lower order vertebrate and invertebrate organisms (Nawabi *et al.*, 2012). Our data support the finding that injured CNS neurons are endowed with an intrinsic ability to regrow dendrites and can readily re-establish functional dendritic arbours upon insulin signalling.

Our data show that insulin-dependent activation of both mTORC1 and mTORC2 is required for dendrite regeneration, and these complexes cooperate in an additive manner to ensure successful restoration of dendritic length and arbour complexity. Intriguingly, our siRNA-mediated loss-of-function experiments revealed that mTORC1 and mTORC2 do not control the same aspects of dendrite regeneration. mTORC1 was required for branching and the restoration of arbour complexity, while mTORC2 regulated process extension and the re-establishment of arbour area. Of interest, partial raptor knockdown had a striking effect on dendritic branching confirming the importance of raptor within the mTORC1 complex. Indeed, raptor forms

Figure 4 Continued

co-localized voxels, which measured the 3D volume occupied by both VGLUT1 and PSD95 in the inner plexiform layer, confirmed that insulin promoted synaptic marker regeneration (insulin: red bar, vehicle: grey bar, ANOVA, $^{***}P < 0.001$, $n = 4$–6 mice/group). (**G**) Representative examples of biolistically labelled RGCs with plasmids encoding tdTomato (red, RGC dendrites) and PSD95-YFP (cyan, PSD95 puncta) at 7 days after axotomy. In the absence of treatment, many retraction bulbs and varicosities (yellow arrowheads) as well as abnormally large PSD95 puncta (white arrowheads) were observed. (**H** and **I**) Higher magnification of dendritic branch segments show abnormally large PSD95 clusters in vehicle-treated retinas relative to intact RGCs. (**J**–**U**) Analysis of 3D-reconstructed PSD95 puncta density along RGC dendrites demonstrated striking insulin-mediated regeneration of excitatory postsynaptic sites in ON-sustained, OFF-sustained, and OFF-transient alpha RGCs relative to vehicle-treated controls. (**J'**–**T'**) Higher magnification images of individual segments are provided to show PSD95-YFP puncta (blue) along dendrites (red) for each condition. Values are expressed as the mean ± SEM. (ANOVA, $^{***}P < 0.001$, $^{**}P < 0.01$, $n = 5$–6 mice/group, $n = 3$–6 RGCs/group). Scale bars: **A**–**C** and **G** = 10 μm, **D** and **E** = 5 μm, **H** and **I** = 1 μm, **J**–**S** = 30 μm, **J'**–**T'** = 2.5 μm. GCL = ganglion cell layer; INL = inner nuclear layer.

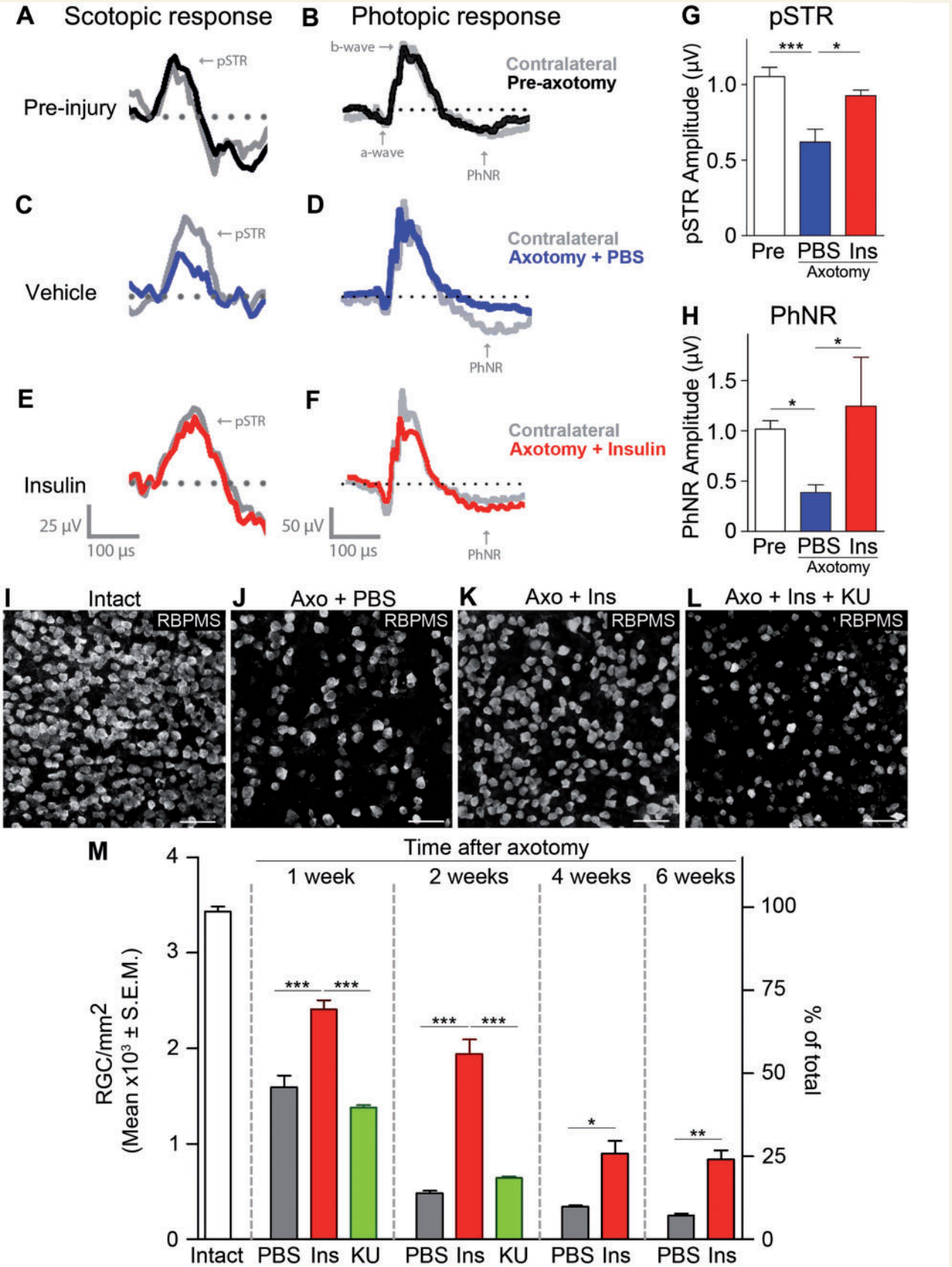

Figure 5 Insulin rescues retinal function and increases neuronal survival. (**A**–**F**) Representative examples of ERG recordings elicited by dim scotopic (**A**, **C** and **E**) or photopic (**B**, **D** and **F**) light stimulation prior to axotomy (pre-injury, black trace), or after axotomy and treatment with PBS (blue trace) or insulin (red trace). Pre- and post-axotomy recordings were normalized relative to the contralateral, non-injured eye (grey traces).

(continued)

a stoichiometric complex with mTOR tightly regulating its kinase activity (Kim *et al.*, 2002), thus a small change in raptor function is expected to have a large impact on mTORC1-mediated dendritic branching. Our finding that mTORC1 mediates insulin-induced branching in RGCs is consistent with developing hippocampal neurons in which mTORC1 inhibition reduces the number of dendritic branches and arbour complexity (Jaworski *et al.*, 2005). This response was mimicked by p70 ribosomal S6 kinase knockdown (Jaworski *et al.*, 2005), thus it is tempting to speculate that mTORC1 controls the addition of new branches during insulin-induced regeneration through activation of protein translation. Consistent with our observation that mTORC2 mediates dendrite extension, Rictor-deficient Purkinje cells lacking mTORC2 have shorter dendrites and decreased arbour area (Thomanetz *et al.*, 2013). In neurons, mTORC2 controls actin polymerization for neuronal shape modification and synaptic plasticity required for the consolidation of long-term memory (Angliker and Rüegg, 2013; Huang *et al.*, 2013; Thomanetz *et al.*, 2013). Therefore, mTORC2 might promote dendrite regenerative growth through regulation of cytoskeleton dynamics.

Deletion of phosphatase and tensin homolog (PTEN), the negative regulator of PI3K upstream of mTOR, enhances axonal regeneration in rodent RGCs and corticospinal neurons, as well as sensory neurons in flies (Park *et al.*, 2008; Liu *et al.*, 2010; Song *et al.*, 2012). Mutations in PTEN also stimulate dendrite regrowth after dendrotomy in *Drosophila* sensory neurons (Song *et al.*, 2012). These findings, together with the data presented here, support a key role of mTOR signalling in both axon and dendrite regeneration after injury. However, our study also highlights important differences in the intrinsic mechanisms used for dendrite versus axonal regeneration in adult RGCs. First, successful dendrite regeneration depends on both mTORC1 and mTORC2 activation (our data), while axonal regeneration requires primarily mTORC1 (Park *et al.*, 2010; Duan *et al.*, 2015), with mTORC2 being growth inhibitory (Miao *et al.*, 2016). Second, we show that insulin-mediated mTORC1/2 activation is sufficient for dendritic regrowth and reconnection to presynaptic targets, whereas mTOR enhancement alone is not enough for RGC axons to reach their brain targets and re-establish functional synapses (Sun *et al.*, 2011; de Lima *et al.*, 2012; Lim *et al.*, 2016). For example, mTOR activation must be combined with approaches that increase neuronal activity, such as high-contrast visual stimulation, to achieve long-distance RGC axon regeneration and target-specific connections (Lim *et al.*, 2016). It is likely that RGC dendrites being in the more growth-permissive retinal environment, relative to the optic nerve, and in closer proximity to their targets require regeneration over shorter distances facilitating the restoration of functional connections. A better understanding of the molecular interplay between dendrite and axon regeneration will be important to design strategies that result in complete circuit restoration.

We show that axonal injury leads to dendrite degeneration and rapid synapse disassembly. Axotomized RGC dendrites display varicosities, retraction bulbs, and larger PSD95 clusters, similar to inactive synapses observed during retinal development (Okawa *et al.*, 2014). Recent studies suggest that RGCs with dendritic stratification in the OFF sublamina are more vulnerable to synaptic alterations in mouse models of ocular hypertension glaucoma (Della Santina *et al.*, 2013; El-Danaf and Huberman, 2015; Ou *et al.*, 2016). However, our finding that OFF and ON alpha RGCs are similarly affected after axotomy suggests that subtype vulnerability depends on injury modality. Remarkably, insulin treatment rescued excitatory postsynaptic sites on RGC dendrites, independently of subtype. In addition to rescuing synaptic inputs, insulin restored the ability of regenerating RGCs to respond to light stimulation restoring circuit function after axonal damage.

Our observation that insulin leads to mTORC1/2-dependent RGC survival after axotomy suggests that increased connectivity with presynaptic targets increases neuronal activity, which might subsequently enhance cell viability. The transient insulin regimen used here, initiated after dendrite retraction and synapse disassembly, promoted ~60% RGC survival at 2 weeks post-axotomy, a time when only 10% of these neurons remained alive in vehicle-treated animals. Insulin-mediated survival was higher than that observed with single or multiple injections of brain-derived neurotrophic factor (BDNF) or insulin growth factor (IGF1), which promoted 38–45% or 20–28% survival, respectively, at 2 weeks after optic nerve injury (Kermer *et al.*, 2000; Cheng *et al.*, 2002; Galindo-Romero *et al.*, 2013; Duan *et al.*, 2015). Analysis of neuronal survival at longer time points after

Figure 5 Continued

(**G** and **H**) Quantitative analysis of the pSTR or PhNR amplitudes demonstrated restoration of RGC function in insulin-treated eyes relative to controls that received vehicle at 7 days post-axotomy (ANOVA, $^{**}P < 0.01$, $^{*}P < 0.05$, $n = 4$–6 mice/group). (**I**–**K**) Flat-mounted retinas from eyes treated with insulin displayed higher densities of RBPMS-positive RGCs compared to control retinas treated with vehicle at 1 week after optic nerve axotomy. (**L**) Co-administration of insulin with KU0063794 completely abrogated the pro-survival effect of insulin, strongly suggesting a role for both mTORC1 and mTORC2 in insulin-mediated RGC survival. Scale bars = 50 μm. (**M**) Quantitative analysis of RBPMS-positive cells confirmed that insulin (red) promoted significant RGC soma survival at 1, 2, 4, and 6 weeks after optic nerve lesion compared to control eyes treated with vehicle (grey), or a combination of insulin and KU0063794 (green). The densities of RGC soma in intact, non-injured animals is shown as reference (white, 100% survival). Systemic administration of KU0063794 alone did not induce RGC death in intact retinas ruling out any toxic effect of this compound. Values are expressed as the mean ± SEM. (ANOVA, $^{***}P < 0.001$, $^{**}P < 0.01$, $^{*}P < 0.05$, $n = 5$–6 mice/group).

axotomy demonstrated that 25% of RGCs survived at 4 and 6 weeks, respectively, relative to only ~8% in vehicle-treated controls. Although still significant, the gradual decrease in RGC survival after 2 weeks is likely to reflect the transient nature of the insulin treatment used here. It should be of future interest to examine the neuroprotective effect of chronic insulin administration on RGC viability after axonal injury. Among RGC subtypes, alpha cells appear to have a greater capacity to survive after axotomy (Duan *et al.*, 2015). However, the high survival rate observed here suggests that other RGC subtypes are likely to be insulin responders. Previous studies have reported subtype-specific alterations in dendritic morphology after optic nerve injury (Thanos, 1988; Watanabe *et al.*, 1995; Leung *et al.*, 2011; Liu *et al.*, 2014; Pérez de Sevilla Müller *et al.*, 2014; Ou *et al.*, 2016). For example, a recent study showed reduction of dendritic branching and length in αRGCs and melanopsin-positive RGCs after induction of ocular hypertension, while ON direction-selective RGCs showed no changes (El-Danaf and Huberman, 2015), suggesting differential responses among subtypes. A detailed characterization of dendritic alterations in distinct RGC types relative to their ability to regenerate and/or survive should expand our understanding of injury-induced responses in the retina.

In summary, this study reveals that adult retinal neurons are endowed with the ability to effectively regenerate dendrites and synapses after injury. We identify insulin, through mTORC1 and mTORC2 signalling, as a powerful strategy to restore dendritic morphology thus enhancing the function and survival of injured neurons. The observation that insulin eye drops exert a potent pro-regenerative effect is reinforced by findings that insulin applied at doses as high as 100 U/ml, several-fold higher than those tested here, were innocuous and produced no detectable clinical toxicity when applied topically in humans (Bartlett *et al.*, 1994). In this regard, it will be of interest to assess whether there is a correlation between glaucoma progression and insulin intake in such patients affected by diabetes. Collectively, these data support the rationale for using insulin and its analogues as pro-regenerative therapeutic targets that are potentially applicable to glaucoma and a host of other intractable neurodegenerative diseases.

Acknowledgements

We thank Drs Lieve Moons (KU Leuven, Belgium) and Timothy Kennedy (Montreal Neurological Institute, McGill University) for critical reading of the manuscript.

Funding

This work was supported by grants from the Glaucoma Research Foundation (San Francisco, California, US) and the Canadian Institutes of Health Research (ADP, grant MOP-125966), and the National Institutes of Health (EY17101 to R.O.L.W. and the vision core grant EY01730).

Supplementary material

Supplementary material is available at *Brain* online.

References

Agostinone J, Di Polo A. Retinal ganglion cell dendrite pathology and synapse loss: implications for glaucoma. Prog Brain Res 2015; 220: 199–216.

Aguayo AJ, Bray GM, Carter DA, Villegas-Perez MP, Vidal-Sanz M, Rasminsky M. Regrowth and connectivity of injured central nervous system axons in adult rodents. Acta Neurobiol Exp 1990; 50: 381–9.

Alarcón-Martínez L, Avilés-Trigueros M, Galindo-Romero C, Valiente-Soriano J, Agudo-Barriuso M, Villa Pdl, et al. ERG changes in albino and pigmented mice after optic nerve transection. Vision Res 2010; 50: 2176–87.

Angliker N, Rüegg MA. *In vivo* evidence for mTORC2-mediated actin cytoskeleton rearrangement in neurons. Bioarchitecture 2013; 3: 113–18.

Athauda D, Foltynie T. Insulin resistance and Parkinson's disease: a new target for disease modification? Prog Neurobiol 2016; 145–6: 98–120.

Baden T, Berens P, Franke K, Román Rosón M, Bethge M, Euler T. The functional diversity of retinal ganglion cells in the mouse. Nature 2016; 529: 345–50.

Bartlett J, Slusser T, Turner-Henson A, Singh K, Atchison J, Pillion D. Toxicity of insulin administered chronically to human eye *in vivo*. J Ocul Pharmacol 1994; 10: 101–7.

Bedse G, Di Domenico F, Serviddio G, Cassano T. Aberrant insulin signaling in Alzheimer's disease: current knowledge. Front Neurosci 2015; 9: 204.

Benowitz LI, He Z, Goldberg JL. Reaching the brain: advances in optic nerve regeneration. Exp Neurol 2017; 287 (Pt 3): 365–73.

Bleckert A, Schwartz GW, Turner MH, Rieke F, Wong RO. Visual space is represented by nonmatching topographies of distinct mouse retinal ganglion cell types. Curr Biol 2014; 24: 310–15.

Bloom GS, Lazo JS, Norambuena A. Reduced brain insulin signaling: a seminal process in Alzheimer's disease pathogenesis. Neuropharmacology 2017, in press. doi: 10.1016/j.neuropharm.2017.09.016.

Bu SY, Yu GH, Xu GX. Expression of insulin-like growth factor 1 receptor in rat retina following optic nerve injury. Acta Ophthalmol 2013; 91: e427–31.

Bui BV, Fortune B. Ganglion cell contributions to the rat full-field electroretinogram. J Physiol 2004; 555 (Pt 1): 153–73.

Cheng L, Sapieha P, Kittlerová P, Hauswirth WW, Di Polo A. TrkB gene transfer protects retinal ganglion cells from axotomy-induced death *in vivo*. J Neurosci 2002; 22: 3977–86.

Chrysostomou V, Crowston J. The photopic negative response of the mouse electroretinogram: reduction by acute elevation of intraocular pressure. Invest Ophthalmol Vis Sci 2013; 54: 4691–7.

Chung J, Kuo CJ, Crabtree GR, Blenis J. Rapamycin-FKBP specifically blocks growth-dependent activation of and signaling by the 70 kd S6 protein kinases. Cell 1992; 69: 1227–36.

Cline HT. Dendritic arbor development and synaptogenesis. Curr Opin Neurobiol 2001; 11: 118–26.

Cochran JN, Hall AM, Roberson ED. The dendritic hypothesis for Alzheimer's disease pathophysiology. Brain Res Bull 2014; 103: 18–28.

Coombs J, van der List D, Wang GY, Chalupa LM. Morphological properties of mouse retinal ganglion cells. Neurosci 2006; 140: 123–36.

de Lima S, Koriyama Y, Kurimoto T, Oliveira JT, Yin Y, Li Y, et al. Full-length axon regeneration in the adult mouse optic nerve and partial recovery of simple visual behaviors. Proc Natl Acad Sci USA 2012; 109: 9149–54.

Della Santina L, Inman DM, Lupien CB, Horner PJ, Wong RO. Differential progression of structural and functional alterations in distinct retinal ganglion cell types in a mouse model of glaucoma. J Neurosci 2013; 33: 17444–57.

Dos DS, Ali SM, Kim DH, Guertin DA, Latek RR, Erdjument-Bromage H, et al. Rictor, a novel binding partner of mTOR, defines a rapamycin-insensitive and Raptor-independent pathway that regulates the cytoskeleton. Curr Biol 2004; 14: 1296–302.

Duan X, Qiao M, Bei F, Kim IJ, He Z, Sanes J. Subtype-specific regeneration of retinal ganglion cells following axotomy: effects of osteopontin and mTOR signaling. Neuron 2015; 85: 1244–56.

El-Danaf RN, Huberman AD. Characteristic patterns of dendritic remodeling in early-stage glaucoma: evidence from genetically identified retinal ganglion cell types. J Neurosci 2015; 35: 2329–43.

Fard MA, Afzali M, Abdi P, Yasseri M, Ebrahimi KB, Moghimi S. Comparison of the pattern of macular ganglion cell-inner plexiform layer defect between ischemic optic neuropathy and open–angle glaucoma. Invest Ophthalmol Vis Sci 2016; 57: 1011–16.

Feng G, Mellor RH, Bernstein M, Keller-Peck C, Nguyen QT, Wallace M, et al. Imaging neuronal subsets in transgenic mice expressing multiple spectral variants of GFP. Neuron 2000; 28: 41–51.

Feng L, Zhao Y, Yoshida M, Chen H, Yang JF, Kim TS, et al. Sustained ocular hypertension induces dendritic degeneration of mouse retinal ganglion cells that depends on cell type and location. Invest Ophthalmol Vis Sci 2013; 54: 1106–17.

Freiherr J, Hallschmid M, Frey WH, Brünner YF, Chapman CD, Hölscher C, et al. Intranasal insulin as a treatment for Alzheimer's disease: a review of basic research and clinical evidence. CNS Drugs 2013; 27: 505–14.

Galindo-Romero C, Avilés-Trigueros M, Jiménez-López M, Valiente-Soriano FJ, Salinas-Navarro M, Nadal-Nicolás F, et al. Axotomy-induced retinal ganglion cell death in adult mice: quantitative and topographic time course analyses. Exp Eye Res 2011; 92: 377–87.

Galindo-Romero C, Valiente-Soriano FJ, Jiménez-López M, García-Ayuso D, Villegas-Pérez MP, Vidal-Sanz M, et al. Effect of brain-derived neurotrophic factor on mouse axotomized retinal ganglion cells and phagocytic microglia. Invest Ophthalmol Vis Sci 2013; 54: 974–85.

García-Martínez JM, Moran J, Clarke RG, Gray A, Cosulich SC, Chresta CM, et al. Ku-0063794 is a specific inhibitor of the mammalian target of rapamycin (mTOR). Biochem J 2009; 421 (Pt 1): 29–42.

Ghasemi R, Haeri A, Dargahi L, Mohamed Z, Ahmadiani A. Insulin in the brain: sources, localization and functions. Mol Neurobiol 2013; 47: 145–71.

Grutzendler J, Helmin K, Tsai J, Gan WB. Various dendritic abnormalities are associated with fibrillar amyloid deposits in Alzheimer's disease. Ann NY Acad Sci 2007; 1097: 30–9.

Hara K, Maruki Y, Long X, Yoshino KI, Oshiro N, Hidayat S, et al. Raptor, a binding partner of target of rapamycin (TOR), mediates TOR action. Cell 2002; 110: 177–89.

He Z, Jin Y. Intrinsic control of axon regeneration. Neuron 2016; 90: 437–51.

Heidelberger R, Thoreson WB, Witkovsky P. Synaptic transmission at retinal ribbon synapses. Prog Ret Eye Res 2005; 24: 682–720.

Hong S, Beja-Glasser VF, Nfonoyim BM, Frouin A, Li S, Ramakrishnan S, et al. Complement and microglia mediate early synapse loss in Alzheimer mouse models. Science 2016; 352: 712–16.

Huang W, Zhu PJ, Zhang S, Zhou H, Stoica L, Galiano M, et al. mTORC2 controls actin polymerization required for consolidation of long-term memory. Nat Neurosci 2013; 16: 441–8.

Huberman AD, Manu M, Koch SM, Susman MW, Lutz AB, Ullian EM, et al. Architecture and activity-mediated refinement of axonal projections from a mosaic of genetically identified retinal ganglion cells. Neuron 2008; 59: 425–38.

Ikenoue T, Hong S, Inoki K. Monitoring mammalian target of rapamycin (mTOR) activity. Methods Enzymol 2009; 452: 165–80.

Jacinto E, Loewith R, Schmidt A, Lin S, Rüegg M, Hall A, et al. Mammalian TOR complex 2 controls the actin cytoskeleton and is rapamycin insensitive. Nat Cell Biol 2004; 6: 1122–8.

Jaworski J, Spangler S, Seeburg DP, Hoogenraad CC, Sheng M. Control of dendritic arborization by the phosphoinositide-3'-Kinase–Akt–mammalian target of rapamycin pathway. J Neurosci 2005; 25: 11300–12.

Jefferies HBJ, Fumagalli S, Dennis PB, Reinhard C, Pearson RB, Thomas G. Rapamycin suppresses 5[prime]TOP mRNA translation through inhibition of p70s6k. EMBO J 1997; 16: 3693–704.

Johnson J, Tian N, Caywood MS, Reimer RJ, Edwards RH, Copenhagen DR. Vesicular neurotransmitter transporter expression in developing postnatal rodent retina: GABA and glycine precede glutamate. J Neurosci 2003; 23: 518–29.

Kermer P, Klöcker N, Labes M, Bähr M. Insulin-like growth factor-I protects axotomized rat retinal ganglion cells from secondary death via PI3-K-dependent Akt phosphorylation and inhibition of caspase-3 *in vivo*. J Neurosci 2000; 20: 722–8.

Kim DH, Sarbassov DD, Ali SM, King JE, Latek RR, Erdjument-Bromage H, et al. mTOR interacts with raptor to form a nutrient-sensitive complex that signals to the cell growth machinery. Cell 2002; 110: 163–75.

Kim DH, Sarbassov DD, Ali SM, Latek RR, Guntur KVP, Erdjument-Bromage H, et al. GβL, a positive regulator of the rapamycin-sensitive pathway required for the nutrient-sensitive interaction between raptor and mTOR. Mol Cell 2003; 11: 895–904.

Koleske AJ. Molecular mechanisms of dendrite stability. Nat Rev Neurosci 2013; 14: 536–50.

Kweon JH, Kim S, Lee SB. The cellular basis of dendrite pathology in neurodegenerative diseases. BMB Reports 2017; 50: 5–11.

Lamming DW, Ye L, Katajisto P, Goncalves MD, Saitoh M, Stevens DM, et al. Rapamycin-induced insulin resistance is mediated by mTORC2 loss and uncoupled from longevity. Science 2012; 335: 1638–43.

Lebrun-Julien F, Duplan L, Pernet V, Osswald IK, Sapieha P, Bourgeois P, et al. Excitotoxic death of retinal neurons *in vivo* occurs via a non-cell-autonomous mechanism. J Neurosci 2009; 29: 5536–45.

Leon S, Yin Y, Nguyen J, Irwin N, Benowitz LI. Lens injury stimulates axon regeneration in the mature rat optic nerve. J Neurosci 2000; 20: 4615–26.

Leung CK, Weinreb RN, Li ZW, Liu S, Lindsey JD, Choi N, et al. Long-term *in vivo* imaging and measurement of dendritic shrinkage of retinal ganglion cells. Invest Ophthalmol Vis Sci 2011; 52: 1539–47.

Li ZW, Liu S, Weinreb RN, Lindsey JD, Yu M, Liu L, et al. Tracking dendritic shrinkage of retinal ganglion cells after acute elevation of intraocular pressure. Invest Ophthalmol Vis Sci 2011; 52: 7205–12.

Lim JH, Stafford BK, Nguyen PL, Lien BV, Wang C, Zukor K, et al. Neural activity promotes long-distance, target-specific regeneration of adult retinal axons. Nat Neurosci 2016; 19: 1073–84.

Liu K, Lu Y, Lee JK, Samara R, Willenberg R, Sears-Kraxberger I, et al. PTEN deletion enhances the regenerative ability of adult corticospinal neurons. Nat Neurosci 2010; 13: 1075–81.

Liu M, Guo L, Salt TE, Cordeiro MF. Dendritic changes in rat visual pathway associated with experimental ocular hypertension. Curr Eye Res 2014; 39: 953–63.

Mansour-Robaey S, Clarke DB, Wang YC, Bray GM, Aguayo AJ. Effects of ocular injury and administration of brain-derived neurotrophic factor on survival and regrowth of axotomized retinal ganglion cells. Proc Natl Acad Sci USA 1994; 91: 1632–6.

Miao L, Yang L, Huang H, Liang F, Ling C, Hu Y. mTORC1 is necessary but mTORC2 and GSK3β are inhibitory for AKT3-induced axon regeneration in the central nervous system. Elife 2016; 5: e14908.

Morgan JE, Datta AV, Erichsen JT, Albon J, Boulton ME. Retinal ganglion cell remodelling in experimental glaucoma. Adv Exp Med Biol 2006; 572: 397–402.

Morgan JL, Schubert T, Wong RO. Developmental patterning of glutamatergic synapses onto retinal ganglion cells. Neural Dev 2008; 3: 8.

Morquette B, Morquette P, Agostinone J, Feinstein E, McKinney RA, Kolta A, et al. REDD2-mediated inhibition of mTOR promotes dendrite retraction induced by axonal injury. Cell Death Differ 2015; 22: 612–25.

Nawabi H, Zukor K, He Z. No simpler than mammals: axon and dendrite regeneration in Drosophila. Genes Dev 2012; 26: 1509–14.

Okawa H, Santina LD, Schwartz GW, Rieke F, Wong RO. Interplay of cell-autonomous and non-autonomous mechanisms tailors synaptic connectivity of converging axons *in vivo*. Neuron 2014; 82: 125–37.

Oren-Suissa M, Gattegno T, Kravtsov V, Podbilewicz B. Extrinsic repair of injured dendrites as a paradigm for regeneration by fusion in Caenorhabditis elegans. Genetics 2017; 206: 215–30.

Ou Y, Jo RE, Ullian EM, Wong RO, Della Santina L. Selective vulnerability of specific retinal ganglion cell types and synapses after transient ocular hypertension. J Neurosci 2016; 36: 9240–52.

Pang JJ, Gao F, Wu SM. Light-evoked excitatory and inhibitory synaptic inputs to ON and OFF α ganglion cells in the mouse retina. J Neurosci 2003; 23: 6063–73.

Park KK, Liu K, Hu Y, Kanter JL, He Z. PTEN/mTOR and axon regeneration. Exp Neurol 2010; 223: 45–50.

Park KK, Liu K, Hu Y, Smith PD, Wang C, Cai B, et al. Promoting axon regeneration in the adult CNS by modulation of the PTEN/mTOR pathway. Science 2008; 322: 963–6.

Paveliev M, Fenrich KK, Kislin M, Kuja-Panula J, Kulesskiy E, Varjosalo M, et al. HB-GAM (pleiotrophin) reverses inhibition of neural regeneration by the CNS extracellular matrix. Sci Rep 2016; 6: 33916.

Pavlidis M, Stupp T, Naskar R, Cengiz C, Thanos S. Retinal ganglion cells resistant to advanced glaucoma: a postmortem study of human retinas with the carbocyanine dye DiI. Invest Ophthalmol Vis Sci 2003; 44: 5196–205.

Peichl L. Alpha ganglion cells in mammalian retinae: common properties, species differences, and some comments on other ganglion cells. Vis Neurosci 1991; 7: 155–69.

Pérez de Sevilla Müller L, Sargoy A, Rodriguez AR, Brecha NC. Melanopsin ganglion cells are the most resistant retinal ganglion cell type to axonal injury in the rat retina. PLoS One 2014; 9: e93274.

Ramírez AI, Salazar JJ, de Hoz R, Rojas B, Gallego BI, Salobrar-García E, et al. Macro- and microglial responses in the fellow eyes contralateral to glaucomatous eyes. In: Bagetta G, Nucci C, editors. Progress in brain research. Amsterdam, Netherlands: Elsevier; 2015. p. 155–72.

Rodriguez AR, de Sevilla Müller LP, Brecha NC. The RNA binding protein RBPMS is a selective marker of ganglion cells in the mammalian retina. J Comp Neurol 2014; 522: 1411–43.

Sarbassov DD, Ali SM, Kim DH, Guertin DA, Latek RR, Erdjument-Bromage H, et al. Rictor, a novel binding partner of mTOR, defines a rapamycin-insensitive and raptor-independent pathway that regulates the cytoskeleton. Curr Biol 2004; 14: 1296–302.

Sarbassov DD, Ali SM, Sengupta S, Sheen JH, Hsu PP, Bagley AF, et al. Prolonged rapamycin treatment inhibits mTORC2 assembly and Akt/PKB. Mol Cell 2006; 22: 159–68.

Sarbassov DD, Guertin D, Ali S, Sabatini D. Phosphorylation and regulation of Akt/PKB by the rictor-mTOR complex. Science 2005; 307: 1098–101.

Saxton RA, Sabatini DM. mTOR signaling in growth, metabolism, and disease. Cell 2017; 168: 960–76.

Schalm SS, Fingar DC, Sabatini DM, Blenis J. TOS motif-mediated Raptor binding regulates 4E-BP1 multisite phosphorylation and function. Curr Biol 2003; 13: 797–806.

Shou T, Liu J, Wang W, Zhou Y, Zhao K. Differential dendritic shrinkage of alpha and beta retinal ganglion cells in cats with chronic glaucoma. Invest Ophthalmol Vis Sci 2003; 44: 3005–10.

Skalecka A, Liszewska E, Bilinski R, Gkogkas C, Khoutorsky A, Malik AR, et al. mTOR kinase is needed for the development and stabilization of dendritic arbors in newly born olfactory bulb neurons. Dev Neurobiol 2016; 76: 1308–27.

Smith BJ, Wang X, Chauhan BC, Côté PD, Tremblay F. Contribution of retinal ganglion cells to the mouse electroretinogram. Doc Ophthalmol 2014; 128: 155–68.

Song BJ, Aiello LP, Pasquale LR. Presence and risk factors for glaucoma in patients with diabetes. Curr Diab Rep 2016; 16: 124.

Song J, Kang SM, Kim E, Kim CH, Song HT, Lee JE. Impairment of insulin receptor substrate 1 signaling by insulin resistance inhibits neurite outgrowth and aggravates neuronal cell death. Neuroscience 2015; 301: 26–38.

Song Y, Ori-McKenney KM, Zheng Y, Han C, Jan LY, Jan YN. Regeneration of Drosophila sensory neuron axons and dendrites is regulated by the Akt pathway involving Pten and microRNA bantam. Genes Dev 2012; 26: 1612–25.

Stephens B, Mueller AJ, Shering AF, Hood SH, Taggart P, Arbuthnott GW, et al. Evidence of a breakdown of corticostriatal connections in Parkinson's disease. Neuroscience 2005; 132: 741–54.

Stone MC, Albertson RM, Chen L, Rolls MM. Dendrite injury triggers DLK-independent regeneration. Cell Rep 2014; 6: 247–53.

Sun F, Park KK, Belin S, Wang D, Lu T, Chen G, et al. Sustained axon regeneration induced by co-deletion of PTEN and SOCS3. Nature 2011; 480: 372–5.

Sun W, Li N, He S. Large-scale morphological survey of mouse retinal ganglion cells. J Comp Neurol 2002; 451: 115–26.

Tham YC, Li X, Wong TY, Quigley HA, Aung T, Cheng CY. Global prevalence of glaucoma and projections of glaucoma burden through 2040: a systematic review and meta-analysis. Ophthalmology 2014; 121: 2081–90.

Thanos S. Alterations in the morphology of ganglion cell dendrites in the adult rat retina after optic nerve transection and grafting of peripheral nerve segments. Cell Tissue Res 1988; 254: 599–609.

Thomanetz V, Angliker N, Cloëtta D, Lustenberger RM, Schweighauser M, Oliveri F, et al. Ablation of the mTORC2 component rictor in brain or Purkinje cells affects size and neuron morphology. J Cell Biol 2013; 201: 293–308.

Thompson-Peer KL, DeVault L, Li T, Jan LY, Jan YN. *In vivo* dendrite regeneration after injury is different from dendrite development. Genes Dev 2016; 30: 1776–89.

Van Wyk M, Wässle H, Taylor WR. Receptive field properties of ON- and OFF-ganglion cells in the mouse retina. Vis Neurosci 2009; 26: 297–308.

Volgyi B, Chheda S, Bloomfield SA. Tracer coupling patterns of the ganglion cell subtypes in the mouse retina. J Comp Neurol 2009; 512: 664–87.

Watanabe M, Sawai H, Fukuda Y. Number and dendritic morphology of retinal ganglion cells that survived after axotomy in adult cats. J Neurobiol 1995; 27: 189–203.

Weber AJ, Kaufman PL, Hubbard WC. Morphology of single ganglion cells in the glaucomatous primate retina. Invest Ophthalmol Vis Sci 1998; 39: 2304–20.

Williams PA, Howell GR, Barbay JM, Braine CE, Sousa GL, John SWM, et al. Retinal ganglion cell dendritic atrophy in DBA/2J glaucoma. PLoS One 2013; 8: e72282.

Wilsey L, Fortune B. Electroretinography in glaucoma diagnosis. Curr Opin Ophthalmol 2016; 27: 118–24.

Wong WT, Wong RO. Rapid dendritic movements during synapse formation and rearrangement. Curr Opin Neurobiol 2000; 10: 118–24.

Yan Z, Kim E, Datta D, Lewis DA, Soderling SH. Synaptic actin dysregulation, a convergent mechanism of mental disorders? J Neurosci 2016; 36: 11411–17.

Zhang H, Berel D, Wang Y, Li P, Bhowmick NA, Figlin RA, et al. A comparison of Ku0063794, a dual mTORC1 and mTORC2 inhibitor, and temsirolimus in preclinical renal cell carcinoma models. PLoS One 2013; 8: e54918.

Zhao Z, Chen S, Luo Y, Li J, Badea S, Ren C, et al. Time-lapse changes of *in vivo* injured neuronal substructures in the central nervous system after low energy two-photon nanosurgery. Neural Regen Res 2017; 12: 751–6.